Gastroenterology 2018;154:1509–1523

Loss of *Pten* and Activation of Kras Synergistically Induce Formation of Intraductal Papillary Mucinous Neoplasia From Pancreatic Ductal Cells in Mice

Janel L. Kopp,[1,2] Claire L. Dubois,[1] David F. Schaeffer,[3] Atefeh Samani,[2] Farnaz Taghizadeh,[2] Robert W. Cowan,[4] Andrew D. Rhim,[4] Bangyan L. Stiles,[5] Mark Valasek,[6] and Maike Sander[1]

[1]*Departments of Pediatrics and Cellular and Molecular Medicine, University of California-San Diego, La Jolla, California;* [2]*Department of Cellular and Physiological Sciences, University of British Columbia, Vancouver, British Columbia, Canada;* [3]*Department of Pathology and Laboratory and Medicine, University of British Columbia, Vancouver, British Columbia, Canada;* [4]*Ahmed Center for Pancreatic Cancer Research and Department of Gastroenterology, Hepatology and Nutrition, University of Texas M.D. Anderson Cancer Center, Houston, Texas;* [5] *Department of Pharmaceutical Sciences, School of Pharmacy, Keck School of Medicine, University of Southern California, and the Norris Comprehensive Cancer Center, Los Angeles, California; and* [6]*Department of Pathology, University of California-San Diego, La Jolla, California*

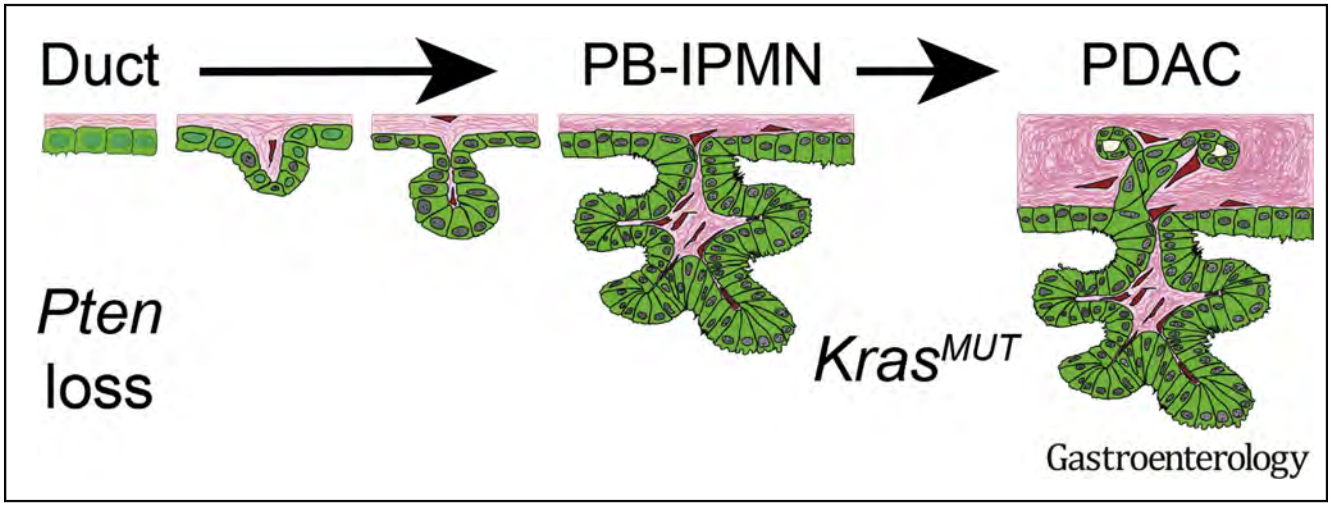

BACKGROUND & AIMS: Intraductal papillary mucinous neoplasias (IPMNs) are precancerous cystic lesions that can develop into pancreatic ductal adenocarcinomas (PDACs). These large macroscopic lesions are frequently detected during medical imaging, but it is unclear how they form or progress to PDAC. We aimed to identify cells that form IPMNs and mutations that promote IPMN development and progression. **METHODS:** We generated mice with disruption of *Pten* specifically in ductal cells ($Sox9CreER^{T2}$;$Pten^{flox/flox}$; $R26R^{YFP}$ or $Pten^{\Delta Duct/\Delta Duct}$ mice) and used $Pten^{\Delta Duct/+}$ and $Pten^{+/+}$ mice as controls. We also generated $Kras^{G12D}$; $Pten^{\Delta Duct/\Delta Duct}$ and $Kras^{G12D}$;$Pten^{\Delta Duct/+}$ mice. Pancreata were collected when mice were 28 weeks to 14.5 months old and analyzed by histology, immunohistochemistry, and electron microscopy. We performed multiplexed droplet digital polymerase chain reaction to detect spontaneous *Kras* mutations in $Pten^{\Delta Duct/\Delta Duct}$ mice and study the effects of Ras pathway activation on initiation and progression of IPMNs. We obtained 2 pancreatic sections from a patient with an invasive pancreatobiliary IPMN and analyzed the regions with and without the invasive IPMN (control tissue) by immunohistochemistry. **RESULTS:** Mice with ductal cell–specific disruption of *Pten* but not control mice developed sporadic, macroscopic, intraductal papillary lesions with histologic and molecular features of human IPMNs. $Pten^{\Delta Duct/\Delta Duct}$ mice developed IPMNs of several subtypes. In $Pten^{\Delta Duct/\Delta Duct}$ mice, 31.5% of IPMNs became invasive; invasion was associated with spontaneous mutations in *Kras*. $Kras^{G12D}$;$Pten^{\Delta Duct/\Delta Duct}$ mice all developed invasive IPMNs within 1 month. In $Kras^{G12D}$;$Pten^{\Delta Duct/+}$ mice, 70% developed IPMN, predominately of the pancreatobiliary subtype, and 63.3% developed PDAC. In all models, IPMNs and PDAC expressed the duct-specific lineage tracing marker yellow fluorescent protein. In immunohistochemical analyses, we found that the invasive human pancreatobiliary IPMN tissue had lower levels of PTEN and increased levels of phosphorylated (activated) ERK compared with healthy pancreatic tissue. **CONCLUSIONS:** In analyses of mice with ductal cell–specific disruption of *Pten*, with or without activated Kras, we found evidence for a ductal cell origin of IPMNs. We also showed that PTEN loss and activated Kras have synergistic effects in promoting development of IPMN and progression to PDAC.

EDITOR'S NOTES

BACKGROUND AND CONTEXT

Intraductal papillary mucinous neoplasia (IPMN) is suggested to arise from the pancreatic ducts, but evidence to directly support this conclusion is lacking.

NEW FINDINGS

Deletion of *Pten* specifically in mouse ductal cells results in IPMN lesions with the potential to progress to pancreatic ductal adenocarcinoma. Additionally, oncogenic Kras combined with PTEN loss is associated with the progression of IPMN to invasive disease.

LIMITATIONS

A larger study is needed to determine how often these events occur in human disease.

IMPACT

The authors generated a mouse model ideal for studying the relevance of IPMN-related allelic variants and demonstrated that Kras and PTEN loss may be indicative of malignant IPMN.

Keywords: Pancreatic Cancer; Oncocytic; PanIN; Gastric.

Pancreatic ductal adenocarcinoma (PDAC) is a highly lethal cancer, with a 5-year survival rate of approximately 9%. PDAC is preceded by the formation of noninvasive premalignant lesions. Based on histological appearance and size, premalignant lesions have been classified into 3 major subtypes, namely microscopic pancreatic intraepithelial neoplasias (PanINs), macroscopic intraductal papillary mucinous neoplasias (IPMNs), and mucinous cystic neoplasias (MCNs). In recent years, the cystic neoplasias (IPMNs and MCNs) have gained attention because improvements in medical imaging have led to higher rates of incidental identification of these lesions.[1] IPMNs comprise 20% to 50% of all pancreatic cystic neoplasms.[1] Although the 5-year survival rate of individuals with noninvasive IPMN is excellent (>77%), the presence of an invasive component drops the 5-year survival rate to 34% to 62%.[1] Currently, the malignant potential of pancreatic cysts is difficult to predict. To enable effective selection for curative surgical intervention, strategies that distinguish benign cysts from lesions with high malignant potential are needed.

An important criterion influencing IPMN prognosis is the location within the pancreatic ductal system. Although branch-duct IPMN has a low risk for malignant progression, individuals with main-duct IPMN are at high risk.[1] The histological IPMN subtype is another prognostic criterion, with intestinal, oncocytic, and gastric IPMN having a more favorable prognosis than pancreatobiliary IPMN.[2,3] However, high-confidence biomarkers to distinguish IPMN with low and high malignant potential or IPMN subtypes are lacking because very little is known about IPMN development.

Several reports have shown that dysregulation of the phosphatidylinositol 3-kinase (PI3K) signaling pathway is associated with IPMN-PDAC compared with conventional PDAC.[4–8] In addition, genetic studies suggest that gastric and pancreatobiliary IPMNs have a higher frequency of *KRAS* mutations than intestinal and oncocytic IPMNs.[9,10] However, the lack of a genetically tractable animal model for IPMNs has hampered studies of how these mutations affect the initiation, progression, or subtype identity of IPMN.

IPMN-like cystic lesions have been observed in several mouse models. For example, $Kras^{G12D}$ (*LSL-Kirsten Rat Sarcoma Viral Oncogene Homolog*^{G12D} allele) expression in combination with *Elastase* promoter-driven transforming growth factor-alpha expression, or loss of Brahma Protein-Like 1 (*Brg1*), *Activin receptor type 1b*, *TIF*γ (Transcriptional Intermediary Factor 1 gamma), or *Smad4* (Mothers Against Decapentaplegic Homolog 4) causes cystic, IPMN-like lesions.[11–15] However, the genetic events in these studies were induced widely in embryonic pancreatic precursors, leading to genetic changes in all pancreatic cells and consequently displacement of most normal pancreatic tissue by cystic and PanIN lesions. The similarity of these mouse models to human IPMNs, where lesions are usually solitary, is limited. Moreover, the pancreas-wide induction of the genetic events precluded studies addressing the cellular origin of the cystic lesions and associated PDAC. von Figura and colleagues[14] recently proposed a ductal origin for IPMN based on their observation that ductal-cell–specific manipulation of *Kras* and *Brg1* induced structures resembling precancerous lesions. However, because these animals could be followed for only 6 weeks, it remained unclear whether these lesions develop into macroscopic IPMN that progress to PDAC. Thus, mouse models fully recapitulating the features of human IPMN and associated PDAC are still missing.

Here, we use ductal-cell–specific manipulation of the PI3K pathway to create a new mouse model that forms macroscopic IPMN lesions of multiple histological subtypes, recapitulating the clinicopathological features of human IPMN. Our analysis of this model provides insight into the cellular origin of IPMN and the subtype-specific genetic mutations that underlie IPMN formation and progression.

Abbreviations used in this paper: ***Brg1***, Brahma Protein-Like 1; IPMN, intraductal papillary mucinous neoplasia; Kras, Kirsten Rat Sarcoma Viral Oncogene Homolog; $Kras^{G12D}$, *LSL-*$Kras^{G12D}$ allele; $Kras^{G12D}$;$Pten^{\Delta Duct/+}$, $Sox9CreER^{T2}$;$Kras^{G12D}$;$Pten^{flox/+}$;$R26R^{YFP}$ mice; $Kras^{G12D}$;$Pten^{\Delta Duct/\Delta Duct}$, $Sox9CreER^{T2}$;$Kras^{G12D}$;$Pten^{flox/flox}$;$R26R^{YFP}$ mice; MCN, mucinous cystic neoplasia; Muc1, Mucin 1; Muc2, Mucin 2; n, sample number; O-IPMN, oncocytic IPMN; PanIN, pancreatic intraepithelial neoplasia; PanIN-PDAC, PanIN-associated PDAC; PB-IPMN, pancreatobiliary IPMN; PB-IPMN-PDAC, pancreatobiliary IPMN-associated PDAC; PCR, polymerase chain reaction; PDAC, pancreatic ductal adenocarcinoma; pErk, phosphorylated Erk; PI3K, phosphatidylinositol 3-kinase; pre-IPMN, microscopic IPMN; pre-O-IPMN, microscopic oncocytic IPMN; pre-PB-IPMN, microscopic pancreatobiliary IPMN; Pten, Phosphatase and Tensin Homolog; $Pten^{+/+}$, $Sox9CreER^{T2}$;$Pten^{+/+}$;$R26R^{YFP}$ mice; $Pten^{\Delta Acinar/+}$, $Ptf1a^{CreER}$;$Pten^{flox/+}$;$R26R^{YFP}$ mice; $Pten^{\Delta Acinar/\Delta Acinar}$, $Ptf1a^{CreER}$;$Pten^{flox/flox}$;$R26R^{YFP}$ mice; $Pten^{\Delta;Duct/+}$, $Sox9CreER^{T2}$;$Pten^{flox/+}$;$R26R^{YFP}$ mice; $Pten^{\Delta Duct/\Delta Duct}$, $Sox9CreER^{T2}$;$Pten^{flox/flox}$;$R26R^{YFP}$ mice; Ptf1a, Pancreas Specific Transcription Factor, 1a; Sox9, SRY (Sex Determining Region Y)-Box 9; TM, Tamoxifen; YFP, yellow fluorescence protein.

Most current article

0016-5085/$36.00
https://doi.org/10.1053/j.gastro.2017.12.007

Methods

Mice

Sox9CreER^{T2},[16] *Ptf1a*^{CreER},[17] *Pten*^{flox},[18] *LSL-Kras*^{G12D},[19] and *R26R*^{YFP} [20] mice have been described previously and were maintained on a mixed C57BL/6 and CD1 background (Charles River Laboratories, Wilmington, MA). Tamoxifen (Sigma-Aldrich, St Louis, MO) was dissolved in corn oil and administered subcutaneously at 5 mg per 40 g of body weight per injection. *Sox9CreER*^{T2};*Pten*$^{flox/+}$;*R26R*^{YFP} (*Pten*$^{\Delta Duct/+}$) and *Sox9CreER*^{T2};*Pten*$^{+/+}$;*R26R*^{YFP} (*Pten*$^{+/+}$) mice were used as controls for *Sox9CreER*^{T2};*Pten*$^{flox/flox}$;*R26R*^{YFP} (*Pten*$^{\Delta Duct/\Delta Duct}$) mice and *Ptf1a*^{CreER};*Pten*$^{flox/+}$;*R26R*^{YFP} (*Pten*$^{\Delta Acinar/+}$) and *Ptf1a*^{CreER};*Pten*$^{+/+}$;*R26R*^{YFP} mice for *Ptf1a*^{CreER};*Pten*$^{flox/flox}$;*R26R*^{YFP} (*Pten*$^{\Delta Acinar/\Delta Acinar}$) mice.

Histology and Immunohistochemical Analysis

Paraffin-embedded sections were subjected to hematoxylin (Mayer's or Harris formulations), eosin, or immunohistochemical staining as described.[21,22] High- or low-resolution scans of entire slides were generated using a Zeiss (Oberkochen, Germany) AxioScan.Z1 or a Zeiss Apoptome microscope, respectively. In combination with necropsy images, whole slide images were used to identify pancreatic duct dilation and presence of papillary nodules/lesions. These images were also used to determine the IPMN subtype, IPMN location, and pre-IPMN and PanIN numbers. Papillary lesions resembling larger IPMN and associated with microscopic, but not macroscopic, duct dilation were classified as a pre-IPMN. Macroscopic tumors associated with lesions in microscopically, but not macroscopically, dilated ducts were classified as pre-IPMN– or PanIN-associated PDAC depending on the presence of papillae. All other microscopic preneoplastic changes in the duct were classified as PanIN.

A list of primary and secondary antibodies used for immunohistochemistry can be found in Supplementary Table 1. The percentage of Ki67-positive cells in large (main and interlobular ducts) and small ducts (intercalated and terminal ducts and centroacinar cells) was quantified from Ki67-stained slides counterstained with hematoxylin. At least 10 ×20 images from each animal were analyzed. Electron microscopy was performed as described.[21] Immunohistochemical staining for phosphorylated Erk was evaluated by estimating the percentage of phosphorylated Erk-positive cells with signal intensity equivalent to a positive control. Strongly positive (+++) lesions had signal in more than 50% of cells, whereas weakly positive samples (+) had signal in fewer than 10% of cells. Moderately positive (++) lesions fell between these criteria. No observed staining was scored as "not detected." All IPMN and pre-IPMN/PanIN lesions in *Pten*$^{\Delta Duct/\Delta Duct}$ mice were analyzed. For Mucin 1 (Muc1), Mucin 2 (Muc2), and Claudin 18 immunohistochemistry, 3 to 15 mice with lesions representing those in the common and main duct were evaluated. Pictures show representative images. PTEN immunohistochemistry signal was scored as "lost" if more than 80% of the cells in the invasive epithelium with atypical nuclear changes did not have signal. This latter distinction was made because PTEN signal was detected in stromal cells and sometimes in the epithelial wall of the cyst.

Allele-Specific Polymerase Chain Reaction (PCR), Droplet Digital PCR, and Tumor Genotyping

Areas of interest were isolated from paraffin-embedded sections using a sterilized razor blade. Nontumor areas and IPMN/PDAC areas were obtained from the same section where possible. Paraffin was removed using xylene, samples were rehydrated, and genomic DNA extracted by heating samples at 55°C overnight in 50-mM Tris-HCl pH 8.0, 20 mM NaCl, 1 mM EDTA pH 8.0, and 1% sodium dodecyl sulfate. DNA was isolated by phenol chloroform extraction using 5-PRIME Phase Lock Gel (FP2302820; Fisher Scientific, Hampton, NH) and DNA concentration determined using NanoDrop (Thermo Scientific, Waltham, MA) or Qubit. The following primers were used to detect the murine *Kras*^{G12D} mutation using allele-specific PCR: wild-type forward primer 5′-ATAAACTTGTGGTGGTTGGAGCTTG-3′; G12D forward primer 5′-ATAAACTTGTGGTGGTTGGAGCTTA-3′; and a common reverse primer 5′-GACTGTAGAGCAGCGTTACC-3′. Primers for the *Pten* allele were used as described.[23]

Mutant *Kras* was quantified using a RainDrop Plus Digital PCR System (RainDance Technologies, Lexington, MA), using a modified version of a described protocol (Pratt et al, unpublished data and Jackson et al[24]). Briefly, DNA (0.88 to 15.9 ng; mean: 5.0 ng) was partitioned into picoliter-sized droplets before a short PCR (98°C for 3 minutes; 9 cycles of 98°C for 10 seconds, 66.5°C for 3 minutes, 72°C for 30 seconds; 72°C for 5 minutes) using Q5 High Fidelity 2x Master Mix (New England Biolabs, Ipswich, MA), 0.5× droplet stabilizer, and 500 nM *Kras*-specific primers (F: AGGCCTGCTGAAAATGACTGAG; R: TGAATTAGCTGTATCGTCAAGGCG) to amplify the input DNA. Amplification was performed within each individual droplet, thereby preserving *Kras* allele frequencies. Droplets were de-emulsified and amplified DNA was isolated using a MiniElute PCR Purification kit (Qiagen, Hilden, Germany) and again partitioned into droplets for PCR (95°C for 10 minutes; 45 cycles of 95°C for 15 seconds, 60°C for 1 minute; 98°C for 10 minutes) using TaqMan Genotyping Master Mix (Applied Biosystems, Foster City, CA), 1× droplet stabilizer, 900 nM of the aforementioned primers, and 100 nM each of *Kras* allele-specific TaqMan probes (wild-type: VIC-TTGGAGCTGGTGGCGT-MGBNFQ; G12C: 6FAM-TGGAGCTTGTGGCGT-MGBNFQ; G12D: 6FAM-TGGAGCTGATGGCGT-MGBNFQ; G12R: 6FAM-TGG AGCTCGTGGCGT-MGBNFQ; G12V: 6FAM-TGGAGCTGTTGGCGT-MGBNFQ). Absolute quantification of wild-type or mutant *Kras*-positive droplets was performed by detecting fluorescence within individual droplets using RainDrop Analyst II software. Baseline was the mean number of mutant droplets in controls and positive mutant populations were defined as those exceeding that mean plus 2 standard deviations.

Statistical Analysis

P values were calculated using the 2-tailed Student *t* test with Excel software (Microsoft Corporation, Redmond, WA).

Study Approval

All animal experiments described herein were approved by the University of California, San Diego Institutional Animal Care and Use Committees (S08215).

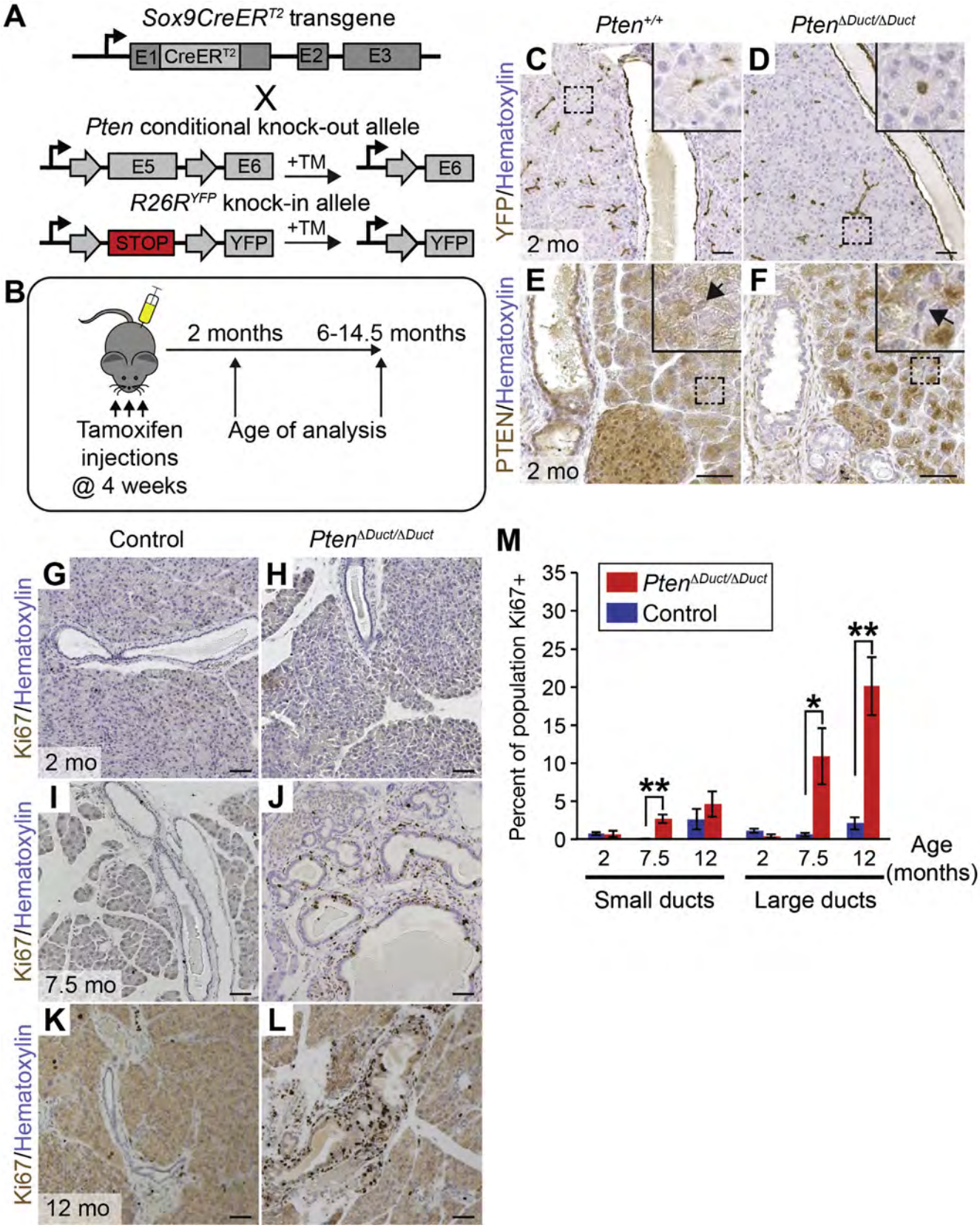
A
Sox9CreER^T2 transgene
E1 CreER^T2 E2 E3
X
Pten conditional knock-out allele
E5 E6 +TM E6
R26R^YFP knock-in allele
STOP YFP +TM YFP
B
2 months
6-14.5 months
Tamoxifen injections @ 4 weeks
Age of analysis
Pten+/+
PtenΔDuct/ΔDuct
C
D
YFP/Hematoxylin
2 mo
E
F
PTEN/Hematoxylin
2 mo
Control
PtenΔDuct/ΔDuct
G
H
Ki67/Hematoxylin
2 mo
I
J
Ki67/Hematoxylin
7.5 mo
K
L
Ki67/Hematoxylin
12 mo
M
PtenΔDuct/ΔDuct
Control
Percent of population Ki67+
35
30
25
20
15
10
5
0
**
*
**
2 7.5 12 2 7.5 12
Age (months)
Small ducts
Large ducts

Results

Loss of Pten in Pancreatic Ductal Cells Leads to Macroscopic Cystic IPMN Lesions

To test whether PTEN plays a role in IPMN formation, we used a genetic strategy to inducibly ablate *Pten* specifically in pancreatic ductal cells of mice. To simultaneously follow the fate of recombined cells that lost PTEN, tamoxifen-inducible *Sox9CreER*^{T2} mice[16] were crossed with mice harboring a Cre-recombinase–dependent yellow fluorescence protein (YFP) reporter allele (*R26R*^{YFP})[20] and a "floxed" allele of the *Pten* gene[18] to generate *Sox9CreER*^{T2};*Pten*$^{flox/flox}$;*R26R*^{YFP} (*Pten*$^{\Delta Duct/\Delta Duct}$), *Sox9CreER*^{T2};*Pten*$^{flox/+}$;*R26R*^{YFP} (*Pten*$^{\Delta Duct/+}$), and *Sox9CreER*^{T2};*Pten*$^{+/+}$;*R26R*^{YFP} mice (*Pten*$^{+/+}$) (Figure 1*A*). At 4 weeks of age, mice were injected 3 times with tamoxifen to induce recombination of the *Pten* floxed allele and expression of YFP (Figure 1*B*). At 1 month after tamoxifen injection, we observed widespread expression of YFP in large ducts, small ducts, and centroacinar cells (Figure 1*C* and *D*, centroacinar cells, insets). As expected, PTEN expression was lost throughout the ductal tree of *Pten*$^{\Delta Duct/\Delta Duct}$ mice, including centroacinar cells (Figure 1*E* and *F*, centroacinar cells, arrows in insets). These results show that we can efficiently ablate *Pten* in ductal cells.

To determine the effect of ductal *Pten* loss, we examined pancreata of 2.0- to 14.5-month-old *Pten*$^{\Delta Duct/\Delta Duct}$ mice. The first noticeable histological change was detected at 6.0 to 7.5 months of age, when we observed hyperplasia in large sections of the main and large ducts in *Pten*$^{\Delta Duct/\Delta Duct}$ mice (Supplementary Figure 1*A* and *B*). To examine whether increased ductal cell proliferation caused large duct hyperplasia in the absence of *Pten*, we quantified the percentage of proliferating cells located in large and small ducts at 2.0, 7.5, and 12.0 months of age in *Pten*$^{\Delta Duct/\Delta Duct}$ and control mice using immunohistochemistry against Ki67 (Figure 1*G–L*). At 7.5 months of age, the proliferation index of large ducts was 18-fold higher in *Pten*$^{\Delta Duct/\Delta Duct}$ than control mice and remained 10-fold higher at 12 months of age (Figure 1*M*). *Pten* loss had less of an effect on small duct cell proliferation (Figure 1*M*). Consistent with this observation, electron microscopy of pancreata at 7.5 months revealed no expansion of the centroacinar/terminal ductal cell compartment in *Pten*$^{\Delta Duct/\Delta Duct}$ mice (Supplementary Figure 1*C* and *D*, arrows). Thus, loss of *Pten* in ductal cells leads to proliferation and hyperplasia predominantly of large ducts.

To examine whether the observed ductal hyperplasia in 6- to 7-month-old *Pten*$^{\Delta Duct/\Delta Duct}$ mice was associated with neoplasia, we examined a large cohort of *Pten*$^{\Delta Duct/\Delta Duct}$ (n = 43), *Pten*$^{\Delta Duct/+}$ (n = 27), and *Pten*$^{+/+}$ (n = 34) mice at 6.0 to 14.5 months. At necropsy, we observed that the main pancreatic duct and/or common duct was visibly enlarged and dilated in 15 of 43 *Pten*$^{\Delta Duct/\Delta Duct}$ mice (Figure 2*A* and *B*, arrows point to area of main duct). This phenotype was not observed in any of the 61 *Pten*$^{\Delta Duct/+}$ and *Pten*$^{+/+}$ mice. In these 15 *Pten*$^{\Delta Duct/\Delta Duct}$ mice, the cross-sectional diameters of the dilated pancreatic and common ducts ranged from 438 to 2800 μm compared with 125 μm for the main pancreatic duct and 150 to 230 μm for the common duct in control mice (Figure 2*Ci,Cii* and *Di,Dii*). The dilated ducts in *Pten*$^{\Delta Duct/\Delta Duct}$ mice displayed papillae or nodules with fibrovascular cores (Figure 2*Dii*, insets; Figure 2*E* and *F;* and Table 1). These papillae and nodules were macroscopically visible, were continuous with the ductal epithelium (Figure 2*Dii*, insets; Figure 2*F*, arrow), lacked the characteristic estrogen-receptor–positive ovarian-type stroma associated with MCN (Supplementary Figure 2*A* and *B*), and had mucinous secretions (Supplementary Figure 2*C*). The focal nature of these macroscopic lesions and their sporadic occurrence in only 34% of *Pten*$^{\Delta Duct/\Delta Duct}$ mice suggests a secondary clonal event leading to expansion of cells within the *Pten*-negative ductal epithelium. Collectively, the features observed in pancreata from *Pten*$^{\Delta Duct/\Delta Duct}$ mice recapitulated hallmarks of human main duct IPMN, namely dilation of the main duct and grossly visible, focal papillary lesions contiguous with the main duct.[1] Based on these similarities, we classified the lesions in *Pten*$^{\Delta Duct/\Delta Duct}$ mice as main duct or common duct IPMN (Table 1).

IPMN Lesions in *Pten*$^{\Delta Duct/\Delta Duct}$ Mice Represent 2 IPMN Subtypes

Morphological differences have led to the classification of human IPMNs into different subtypes.[1] The papillae in *Pten*$^{\Delta Duct/\Delta Duct}$ mice had 2 morphologically different appearances, suggesting different subtype identity. One type of papillae exhibited a complex arborizing morphology with predominantly single-cell–layered epithelium reminiscent of human pancreatobiliary IPMN (Figure 2*Dii*, PB-IPMN; Figure 2*E*). The other type was composed of tightly packed, multiple-cell–layered epithelial folds containing cells with eosinophilic, granular cytoplasm and distinct nucleoli (Figure 2*Dii*, O-IPMN; Figure 2*F*), similar to human oncocytic IPMN. Typically, only 1 subtype was present in an individual animal;

Figure 1. *Pten* deletion in pancreatic ductal cells increases cell proliferation in large ducts. (*A*) Strategy to generate *Sox9CreER*^{T2};*Pten*$^{flox/flox}$;*R26R*^{YFP} (*Pten*$^{\Delta Duct/\Delta Duct}$), *Sox9CreER*^{T2};*Pten*$^{flox/+}$;*R26R*^{YFP} (*Pten*$^{\Delta Duct/+}$), and *Sox9CreER*^{T2};*Pten*$^{+/+}$;*R26R*^{YFP} (*Pten*$^{+/+}$) mice. TM injection induces recombination of *Pten*^{flox} and *R26R*^{YFP} alleles in *Sox9*-expressing cells. (*B*) *Pten*$^{\Delta Duct/\Delta Duct}$, *Pten*$^{\Delta Duct/+}$, and *Pten*$^{+/+}$ mice were injected with TM on postnatal days 28, 30, and 32 and analyzed at 2.0 or 6.0 to 14.5 months of age. (*C–F*) Immunohistochemistry for YFP (*C, D*) and PTEN (*E, F*) in 2-month-old *Pten*$^{+/+}$ and *Pten*$^{\Delta Duct/\Delta Duct}$ mice. Insets show centroacinar/terminal duct cells (arrows in *E, F*). (*G–L*) Immunohistochemistry for Ki67 in 2.0- (*G, H*), 7.5- (*I, J*), and 12.0-month-old (*K, L*) control and *Pten*$^{\Delta Duct/\Delta Duct}$ mice. (*M*) Quantification of Ki67^{+} cells in small and large ducts in control and *Pten*$^{\Delta Duct/\Delta Duct}$ mice (n = 3). Values are shown as mean ± SEM. **P* < .05 and ***P* < .01. Scale bars: 50 μm (*C–L*).

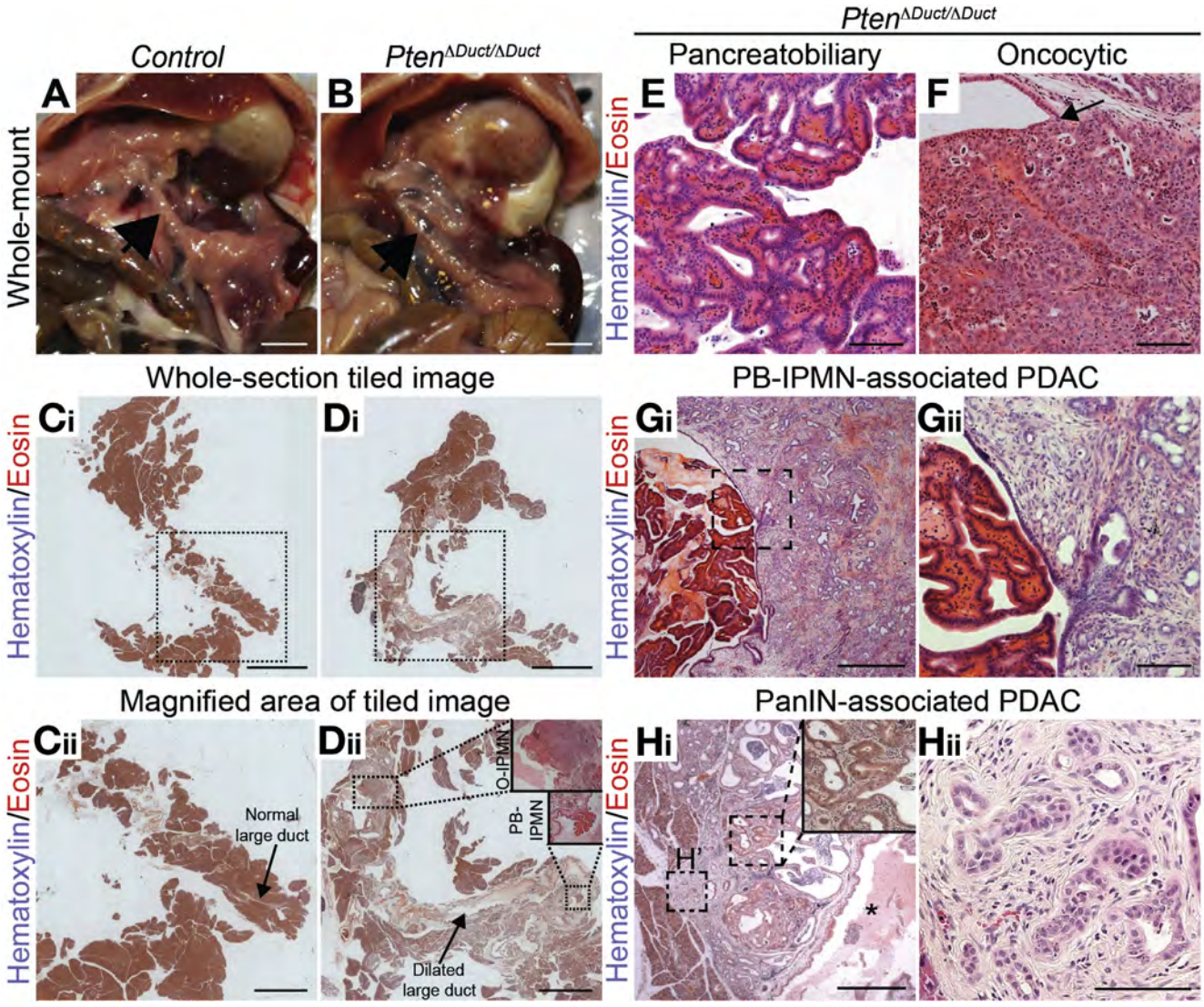

Figure 2. *Pten* deletion in pancreatic ductal cells causes invasive macroscopic IPMN lesions. (*A, B*) In situ image showing the main pancreatic duct (arrow) in control or $Pten^{\Delta Duct/\Delta Duct}$ mice. (*C–H*) Hematoxylin/eosin staining of pancreatic sections from control and $Pten^{\Delta Duct/\Delta Duct}$ mice. Outlined areas in *Ci* and *Di* are magnified in *Cii* and *Dii*, respectively. Arrows in *Cii* and *Dii* indicate the main pancreatic duct. IPMN of oncocytic (O-IPMN) and pancreatobiliary (PB-IPMN) subtypes are outlined and magnified in insets in *Dii*. $Pten^{\Delta Duct/\Delta Duct}$ mice exhibit pancreatobiliary (*E*) and oncocytic (*F*) IPMN, as well as PB-IPMN-associated PDAC (*Gi, Gii*) and PanIN-associated PDAC (*Hi, Hii*). Arrow in *F* points to transition between normal ductal epithelium and the papillary nodule. Outlined areas in *Gi* and *Hi* are magnified in *Gii* and *Hii*, respectively. The inset in *Hi* shows PanIN at high magnification. Asterisk in *Hi* indicates dilated lumen of the main duct. Scale bars: 5 mm (*A–Di*), 2 mm (*Cii, Dii*), 100 μm (*E, F, Gii*, and *Hii*), and 500 μm (*Gi, Hi*).

however, in 1 mouse both subtypes were observed, albeit in distinct foci (Figure 2*Di*; Table 1). Overall, pancreatobiliary IPMN was more common than oncocytic IPMN (15 vs 4 lesions).

To further investigate the similarity of IPMN-like lesions in $Pten^{\Delta Duct/\Delta Duct}$ mice with human oncocytic and pancreatobiliary IPMN, we analyzed Muc1 and Muc2 expression. Similar to human pancreatobiliary and oncocytic subtypes, which express Muc1, but not Muc2,[2] both types of papillary lesions in $Pten^{\Delta Duct/\Delta Duct}$ mice were Muc1-positive and Muc2-negative (Supplementary Figure 2*D–G*). We further confirmed the preneoplastic nature of these lesions by showing that lesions of both subtypes express Claudin 18 (Cldn18) (Supplementary Figure 2*H* and *I*), which is expressed in neoplastic lesions but not in normal mouse ductal cells.[25] Together, these data suggest that the PTEN-negative ductal epithelium gives rise to papillae representing the murine counterparts of pancreatobiliary or oncocytic subtypes of human IPMN.

Invasive PDAC Predominantly Associates With Pancreatobiliary IPMN in $Pten^{\Delta Duct/\Delta Duct}$ Mice

As IPMN is a precursor lesion for invasive carcinoma,[1] we next examined whether IPMNs in $Pten^{\Delta Duct/\Delta Duct}$ mice were

Table 1. Characteristics of Pancreatic Lesions in $Pten^{\Delta Duct/\Delta Duct}$ Mice

Mouse ID	Age (months)	IPMN Histology	IPMN Location	Invasive/PDAC	pErk	$Kras^{G12D}$	Pre-IPMN	PanIN
284	14	Oncocytic	C	ND	+[c]	ND	2 Onc	2
58	12	Oncocytic	C	ND	ND	ND	0	2
98	12	Oncocytic	T	Y[a]	ND	ND	0	6
		Pancreatobiliary	H	ND	+	not tested		
64	12	Pancreatobiliary	H, C	Y	+++	Y	0	4
130	12	Pancreatobiliary	T	ND	ND	ND	0	3
132	12	Pancreatobiliary	T	ND	ND	ND	0	3
		Pancreatobiliary	C	Y[a]	ND	ND		
150	12	Pancreatobiliary	C	Y[a]	+++	Y	1 Onc	3
247	13.5	Pancreatobiliary	T	ND	ND	ND	1 PB	7
168	13	Pancreatobiliary	T	Y[a]	+++	Y	0	18[b]
		Pancreatobiliary	H	Y[a]	++	ND		
63	11	Pancreatobiliary	H	ND	+++	ND	1 PB	14[b]
		Pancreatobiliary	H	Y[a]	++	ND		
263	10.5	Pancreatobiliary	C	ND	++	ND	2 PB	5
246	9	Pancreatobiliary	C	ND	ND	ND	1 PB	1
252	7	Pancreatobiliary	C	ND	ND	ND	0	0
93	8	Pancreatobiliary	H, T	ND	+	ND	0	0
24	6	Oncocytic	H, T	ND	+[c]	ND	5 Onc	2

ND, not detected; Y, Present; Onc, oncocytic; IPMN; PB, pancreatobiliary IPMN; Location: H, pancreatic head; T, pancreatic tail; C, common duct.
[a]Denotes microscopic invasive adenocarcinomas.
[b]PanIN3 and associated PDAC observed.
[c]Denotes lesions where pErk signal was present in the epithelial wall of the lesion, but not the papilla.
When more than one mass or lesion was present and these lesions were in distinct locations within the pancreas, they were recorded as separate lesions rather than as a lesion with a mixed phenotype.

associated with PDAC. At necropsy, we observed a mass visible to the naked eye on the wall of the dilated duct in 1 of the 15 $Pten^{\Delta Duct/\Delta Duct}$ mice with grossly visible IPMN. Histological analysis revealed well-differentiated PDAC directly contiguous with a pancreatobiliary-type IPMN (Figure 2*Gi,Gii*), suggesting IPMN progression to invasive carcinoma. In addition to the

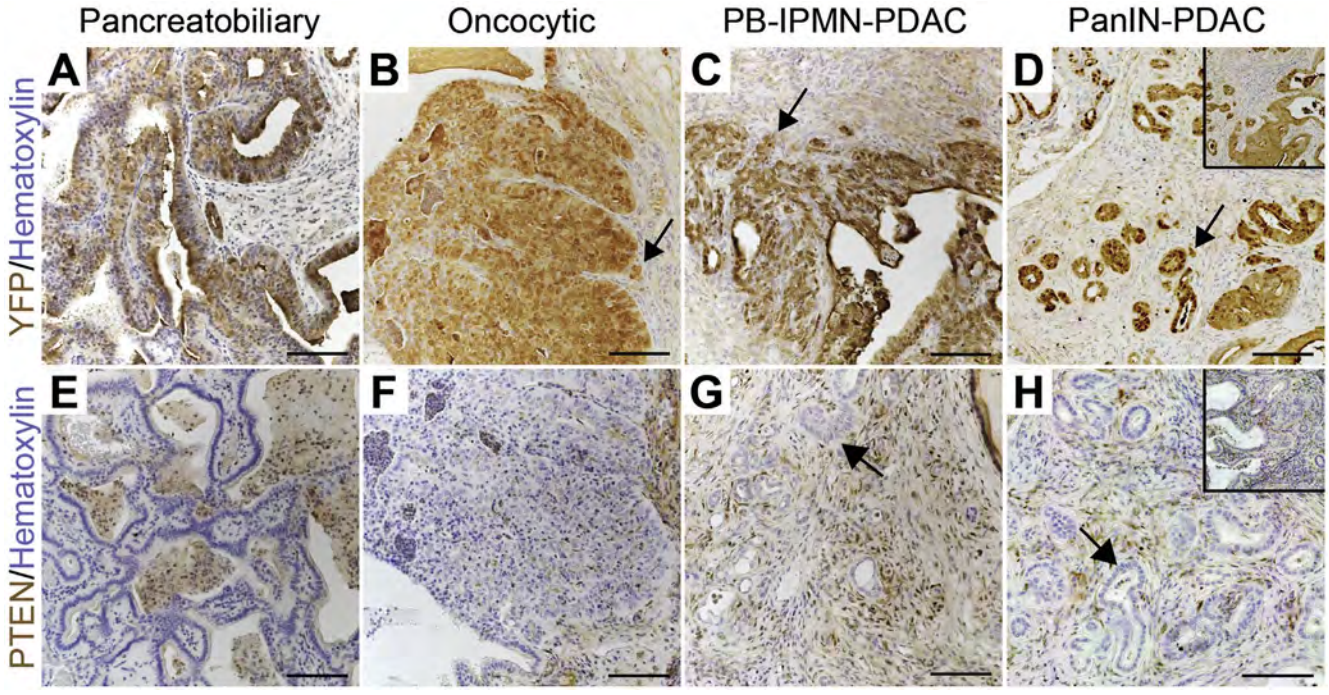

Figure 3. IPMN and associated PDAC originate from ductal cells. Immunohistochemistry for YFP (*A–D*) and PTEN (*E–H*) in pancreatobiliary IPMN (*A, E*), oncocytic IPMN (*B, F*), pancreatobiliary IPMN-associated PDAC (PB-IPMN-PDAC) (*C, G*), and PanIN-associated PDAC (PanIN-PDAC) (*D, H*). Insets in *D* and *H* depict PanIN. Arrows in (*B–D* and *G, H*) denote invasive cells. Scale bars: 100 μm.

1 macroscopic PDAC, we observed small microscopic invasive tumors or cellular invasion directly associated with 5 pancreatobiliary and 1 oncocytic IPMN in *Pten*$^{\Delta Duct/\Delta Duct}$ mice (Table 1). Thus, as in human IPMN,[1] a higher percentage of pancreatobiliary compared with oncocytic IPMN became invasive in *Pten*$^{\Delta Duct/\Delta Duct}$ mice.

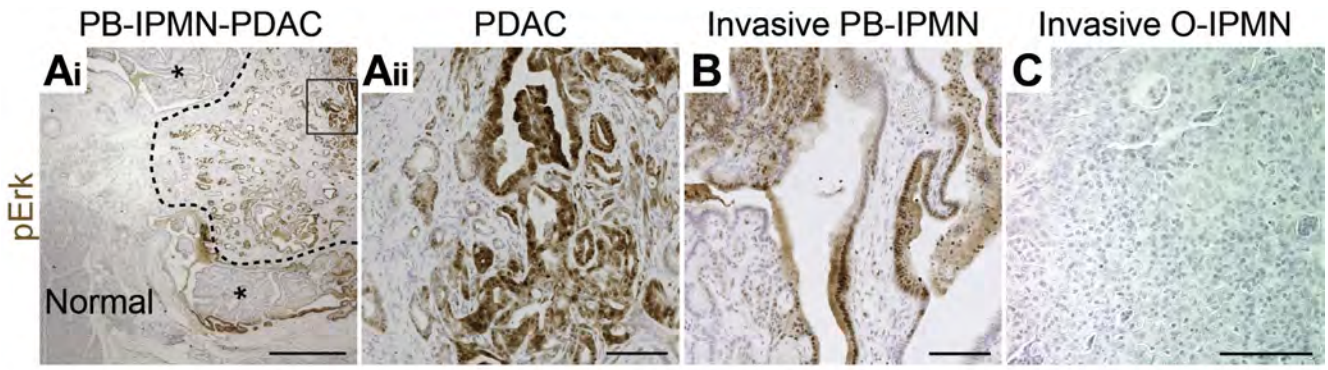

D

Mouse ID	IPMN histology	IPMN location	Number of *Kras* mutant alleles (% of total *Kras*)	
			Normal area	IPMN/PDAC area
64	PB*	C	129 (0.095)	10625 (9.765) (G12C>G12D)
168	PB*	T	38 (0.044)	4209 (9.320) (G12D)
284	Oncocytic	C	116 (0.118)	765 (6.005)
132	PB*	C	19 (0.062)	328 (0.082)
263	PB	C	42 (0.123)	164 (3.017)
98	Oncocytic*	T	54 (0.078)	70 (0.423)
130	PB	T	11 (0.043)	55 (0.574)
63	PB*	H	66 (0.095)	46 (0.019)
93	PB	T, H	1 (0.010)	2 (0.002)

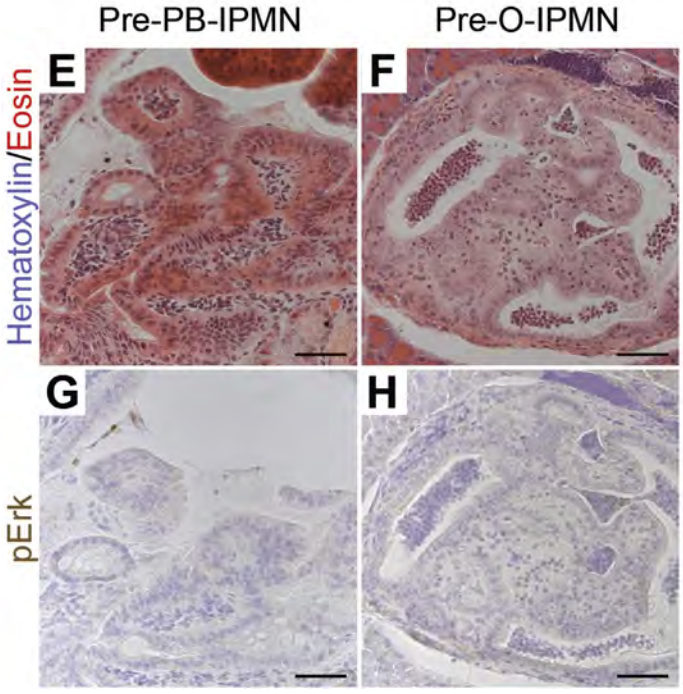

In 2 mice with IPMN, microscopic tumors distant from the IPMN were also observed (Figure 2*Hi,Hii*). These small well-differentiated tumors were directly adjacent to large ducts with an inflammatory reactive atypia that transitioned into epithelium with PanIN features (Figure 2*Hi*, inset; Table 1, mice #63 and #168). This resembles human IPMN-PDAC, where PDAC can be found in regions distinct from the IPMN.[3] Because we observed PanIN-associated PDAC only in mice with IPMN (Table 1) and significant main-duct distention and metaplasia, PanIN-associated tumors are likely secondary to main-duct obstruction and the resulting inflammatory response. Together, these data suggest that *Pten* deficiency predisposes ductal cells to malignant transformation, manifesting in IPMN-associated and distant PDAC similar to human IPMN-PDAC.

IPMN-Associated PDAC in $Pten^{\Delta Duct/\Delta Duct}$ Mice Arises From Ductal Cells

To determine whether IPMN-PDAC in $Pten^{\Delta Duct/\Delta Duct}$ mice originated from ductal cells, we examined whether the precursor lesions and tumors expressed YFP, and lacked PTEN protein. Consistent with a ductal origin of these lesions, pancreatobiliary- (Figure 3*A* and *E*) and oncocytic-type IPMN (Figure 3*B* and *F*), as well as the invasive tumors associated with pancreatobiliary IPMN (Figure 3*C* and *G*) in $Pten^{\Delta Duct/\Delta Duct}$ mice were YFP-positive and PTEN-negative. Likewise, PanIN lesions and associated PDAC observed in a subset of $Pten^{\Delta Duct/\Delta Duct}$ mice with IPMN-PDAC expressed YFP and lacked PTEN (Figure 3*D* and *H*, insets show PanIN), showing a ductal origin.

To further confirm that ductal and not pancreatic acinar cells are the origin of IPMN in $Pten^{\Delta Duct/\Delta Duct}$ mice, we generated $Ptf1a^{CreER};Pten^{flox/flox};R26R^{YFP}$ ($Pten^{\Delta Acinar/\Delta Acinar}$) mice (Supplementary Figure 3*A*) to ablate *Pten* in acinar cells. We injected mice with tamoxifen at 4 weeks of age (Supplementary Figure 3*B*), assessed recombination at 4 months of age, and analyzed pancreata for the presence of premalignant lesions or PDAC at 12 to 13 months ($n = 9$). Despite efficient recombination and expression of YFP in the acinar cell compartment (Supplementary Figure 3*C*), pancreatic ducts appeared normal and premalignant lesions were not observed in $Pten^{\Delta Acinar/\Delta Acinar}$ mice (Supplementary Figure 3*D* and *E*). Because hyperplastic ducts and IPMN lesions were observed in $Pten^{\Delta Duct/\Delta Duct}$ mice at 12 months, IPMN lesions in $Pten^{\Delta Duct/\Delta Duct}$ mice are unlikely to arise from acinar cells that ectopically recombined the $Pten^{flox}$ allele. These findings indicate a specific link between PTEN loss in ductal cells and IPMN formation.

Spontaneous *Kras* Mutations Are Associated With Progression of Pancreatobiliary, But Not Oncocytic, IPMN

Genetic studies in patient samples have shown that *KRAS* mutations are preferentially associated with pancreatobiliary- and gastric-type IPMN when compared with intestinal- and oncocytic-type IPMN.[9,10] To further characterize the molecular events associated with the induction of IPMN in $Pten^{\Delta Duct/\Delta Duct}$ mice, we examined phosphorylated Erk (pErk) expression as an indicator of active Ras signaling. Consistent with the higher incidence of *KRAS* mutations in human pancreatobiliary IPMN,[9,10] pErk levels were higher in pancreatobiliary- than oncocytic-type IPMN in $Pten^{\Delta Duct/\Delta Duct}$ mice (Figure 4*A–C*, Supplementary Figure 4*A*, and Table 1). These results suggest that human IPMN and the $Pten^{\Delta Duct/\Delta Duct}$ IPMN mouse model exhibit a similar subtype-specific pattern of Ras signaling activation.

We next examined whether Erk activation was associated with acquisition of spontaneous *Kras* mutations. For this, we first performed allele-specific PCR for the *G12D Kras* mutation, commonly found in human IPMN,[10] on DNA from section areas containing histologically normal tissue, IPMN, or IPMN/PDAC areas in $Pten^{\Delta Duct/\Delta Duct}$ mice. As expected, the wild-type *G12* DNA sequence was amplified from all samples (Supplementary Figure 4*B*). The *G12D* mutation was amplified in samples from pancreatobiliary IPMN lesions, but not normal tissue or oncocytic IPMN (Supplementary Figure 4*B*, lane 8; Table 1). Notably, we detected *Kras G12D* in only 3 of 15 pancreatobiliary IPMN, and all IPMN lesions with this mutation exhibited micro- or macro-invasion (Supplementary Figure 4*B*, lane 4 vs lane 6; Table 1). To further examine whether additional variant alleles for *Kras G12* are present in $Pten^{\Delta Duct/\Delta Duct}$ mice, we performed a more sensitive multiplexed droplet digital PCR with probes to detect the G12D, G12C, G12R, and G12V variant alleles in a subset of samples where sufficient material was left (Figure 4*D* and Supplementary Figure 4*C* and *D*). These analyses confirmed our previous results and additionally indicated that 2 more pancreatobiliary IPMNs were positive for *Kras* mutant alleles, including one that was invasive. We also detected a *Kras* mutation in 1 oncocytic IPMN that had active Erk signaling in the cyst wall (Figure 4*D* and Supplementary Figure 4*A*), suggesting that the cyst wall developed the *Kras* mutation independently of the oncocytic papillary nodule, which was not pErk positive (Supplementary Figure 4*A*). This

Figure 4. Activation of Ras signaling in pancreatobiliary IPMN-PDAC in $Pten^{\Delta Duct/\Delta Duct}$ mice. (*Ai–C*) Immunohistochemistry for pErk on pancreatic sections of 12-month-old $Pten^{\Delta Duct/\Delta Duct}$ mice, showing that PB-IPMN (asterisks in *Ai* and higher magnification in *B*), its associated PDAC (outlined by dashed line in *Ai* and boxed area magnified in *Aii*) are positive, whereas invasive O-IPMN (*C*) is negative. (*D*) Multiplexed droplet digital PCR for *Kras G12* codon variants. Gray-shaded samples are considered positive (>2 standard deviations above the mean level of *Kras* mutations in controls). *Denotes microscopic invasive adenocarcinomas. H, pancreatic head; T, pancreatic tail; C, common duct. (*E–H*) Hematoxylin/eosin (*E, F*) and immunohistochemistry for pErk (*G, H*) displaying microscopic lesions resembling pancreatobiliary (pre-PB-IPMN) (*E, G*) or oncocytic IPMN (pre-O-IPMN) (*F, H*) subtypes in $Pten^{\Delta Duct/\Delta Duct}$ mice. *E* and *G*, as well as *F* and *H*, are adjacent sections. Scale bars: 500 μm (*Ai*), 100 μm (*Aii–C*), and 50 μm (*E–H*).

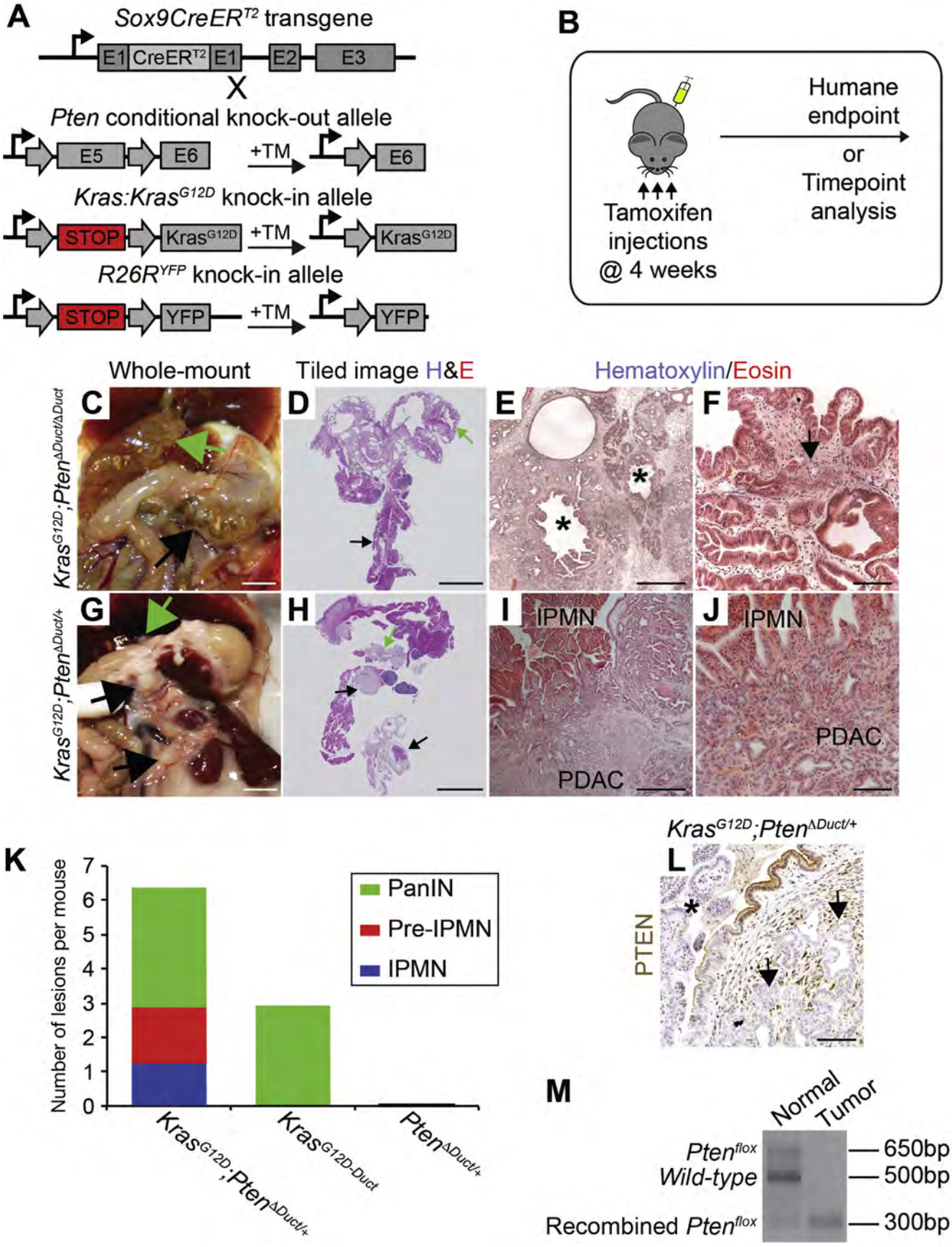
A
Sox9CreER^T2 transgene
E1 CreER^T2 E1 E2 E3
X
Pten conditional knock-out allele
E5 E6 +TM E6
Kras:Kras^G12D knock-in allele
STOP Kras^G12D +TM Kras^G12D
R26R^YFP knock-in allele
STOP YFP +TM YFP
B
Humane endpoint
or
Timepoint analysis
Tamoxifen injections @ 4 weeks
Whole-mount
Tiled image H&E
Hematoxylin/Eosin
Kras^G12D;Pten^ΔDuct/ΔDuct
Kras^G12D;Pten^ΔDuct/+
C
D
E
F
G
H
I
IPMN
PDAC
J
IPMN
PDAC
K
Number of lesions per mouse
0
1
2
3
4
5
6
7
PanIN
Pre-IPMN
IPMN
Kras^G12D;Pten^ΔDuct/+
Kras^G12D-Duct
Pten^ΔDuct/+
Kras^G12D;Pten^ΔDuct/+
L
PTEN
M
Normal
Tumor
Pten^flox
Wild-type
Recombined Pten^flox
650bp
500bp
300bp

raised the possibility that the *Kras* mutations could arise after IPMN initiation and be more important for IPMN progression. In support of this, we detected 2 different *Kras* mutations in the large IPMN-PDAC when the *Kras* variant probes were assayed individually (Figure 4*D*, mouse #64). Moreover, the invasive components of the pancreatobiliary IPMN were often more uniformly pErk-positive than the papillary nodules (Figure 4*Ai*, outlined area vs area denoted with asterisks; Figure 4*Aii* vs 4*B*), implying that Ras activation in the absence of *Pten* can be a late event associated with invasion in the context of pancreatobiliary IPMN. Importantly, no *Kras G12* mutations were detected in the invasive oncocytic IPMN (Figure 4*D* and Supplementary Figure 4*D*, mouse #98). This suggests that, as in human disease, *Kras* mutations are predominantly associated with the development of pancreatobiliary, but not oncocytic IPMN.

To further confirm the link between Ras activation and IPMN progression but not initiation, we examined whether Erk signaling was activated in microscopic precursor lesions potentially preceding IPMN in $Pten^{\Delta Duct/\Delta Duct}$ mice. To investigate this, we analyzed $Pten^{\Delta Duct/\Delta Duct}$ mice devoid of macroscopic IPMN at 6 to 14 months (n = 27). In this cohort, we observed microscopic lesions consisting of single-cell–layered intraductal papillae that were occasionally large enough to contain branched structures (Figure 4*E*, 4 mice with 1 lesion each). Based on their similarity with pancreatobiliary IPMN, we designated these lesions pre-pancreatobiliary-IPMN. A second type of lesion consisted of papillae that had a diffuse eosinophilic cytoplasm and round nuclei randomly localized within the cell (Figure 4*F*, 4 mice with at least 1 lesion). In some cases, these papillae had a dense multilayered epithelium, resembling macroscopic oncocytic IPMN. Therefore, we designated these lesions pre-oncocytic-IPMN. If Ras activation was important for the induction of these microscopic lesions, pErk should be detected. However, neither pre-pancreatobiliary-IPMN nor pre-oncocytic-IPMN (Figure 4*G* and *H*) exhibited the uniformly strong positive pErk staining observed in invasive portions of pancreatobiliary IPMN (Figure 4*Ai,Aii* and *B*). Combined, the absence of pErk in microscopic lesions and the progressive acquisition of pErk signal during the development of pancreatobiliary IPMN-PDAC suggests that Ras activation in $Pten^{\Delta Duct/\Delta Duct}$ mice is a later event during progression of pancreatobiliary IPMN to PDAC.

Oncogenic Kras Promotes IPMN and PDAC Formation in the Absence of Pten

To test whether Kras activation in the absence of *Pten* promotes pancreatobiliary IPMN and its invasion, we crossed *LSL-*$Kras^{G12D}$ mice (hereafter referred to as $Kras^{G12D}$ mice) with $Sox9CreER^{T2}$;$Pten^{flox/flox}$;$R26R^{YFP}$ mice to generate $Sox9CreER^{T2}$;$Kras^{G12D}$;$Pten^{flox/flox}$;$R26R^{YFP}$ ($Kras^{G12D}$;$Pten^{\Delta Duct/\Delta Duct}$) mice (Figure 5*A*). Expression of $Kras^{G12D}$ and ablation of *Pten* was induced by injecting 4-week-old mice 3 times with tamoxifen (Figure 5*B*). To assess IPMN and PDAC formation, we followed $Kras^{G12D}$;$Pten^{\Delta Duct/\Delta Duct}$ mice (n = 14) to their humane endpoint. Within 2 to 4 weeks after tamoxifen administration, $Kras^{G12D}$;$Pten^{\Delta Duct/\Delta Duct}$ mice exhibited weight loss and became moribund. Extensive distension of the common duct was observed in all $Kras^{G12D}$;$Pten^{\Delta Duct/\Delta Duct}$ mice (Figure 5*C*, green arrow), whereas additional dilation of the main pancreatic duct was observed in 10 of 14 mice (Figure 5*C*, black arrow). Analysis of pancreatic sections revealed extensive papillae, resembling IPMN, lining the common duct (Supplementary Figure 5*A*, curved double-headed arrow) and the main and large pancreatic ducts (Figure 5*D* and *E*, asterisks). The peribiliary glands of the common duct were expanded (Supplementary Figure 5*A*, arrow). Consistent with detection of the Kras *G12D* mutation in IPMN-associated PDAC in $Pten^{\Delta Duct/\Delta Duct}$ mice, $Kras^{G12D}$;$Pten^{\Delta Duct/\Delta Duct}$ mice exhibited a fully penetrant phenotype of invasive PDAC (Figure 5*D–F*). The rapid and widespread formation of papillae and invasion along the common and main pancreatic duct suggests that activation of Kras and loss of *Pten* is sufficient to induce invasive IPMN in ductal cells lining the common and main pancreatic ducts.

Pten Reduction and Oncogenic Kras Synergistically Induce Preneoplastic Lesions From Ductal Cells

Expression of $Kras^{G12D}$ alone in ductal cells induces occasional PanIN lesions in a subset of mice by 8 to 16 months,[22] whereas heterozygous loss of *Pten* produced

Figure 5. Synergy between *Pten* reduction and oncogenic Kras in the induction of IPMN-PDAC from ductal cells. (*A*) Strategy to generate $Sox9CreER^{T2}$;$Kras^{G12D}$;$Pten^{flox/flox}$;$R26R^{YFP}$ ($Kras^{G12D}$;$Pten^{\Delta Duct/\Delta Duct}$) and $Sox9CreER^{T2}$;$Kras^{G12D}$;$Pten^{flox/+}$;$R26R^{YFP}$ ($Kras^{G12D}$;$Pten^{\Delta Duct/+}$) mice. TM injection induces recombination of the $Kras^{G12D}$, $Pten^{flox}$, and $R26R^{YFP}$ alleles in *Sox9*-expressing cells. (*B*) $Kras^{G12D}$;$Pten^{\Delta Duct/\Delta Duct}$ and $Kras^{G12D}$;$Pten^{\Delta Duct/+}$ mice were injected with TM on postnatal days 28, 30, and 32 and killed at their humane endpoint or at specific time points, respectively. In situ (*C, G*) and tiled hematoxylin/eosin images (*D, H*) of the pancreas in $Kras^{G12D}$;$Pten^{\Delta Duct/\Delta Duct}$ and $Kras^{G12D}$;$Pten^{\Delta Duct/+}$ mice at 9 weeks and 6 months, respectively. Black arrows denote lesions in the main pancreatic duct and green arrows in the common duct. Representative low- (*E, I*) and high-power (*F, J*) images of hematoxylin/eosin-stained pancreatic sections from $Kras^{G12D}$;$Pten^{\Delta Duct/\Delta Duct}$ and $Kras^{G12D}$;$Pten^{\Delta Duct/+}$ mice. IPMN-like lesions in dilated ducts (asterisks in *E*) are accompanied by PDAC (arrow in *F*). (*K*) Quantification of lesions in 4- to 8-month-old $Kras^{G12D}$;$Pten^{\Delta Duct/+}$ (n = 30; Supplementary Table 1), 8- to 16-month-old $Sox9CreER^{T2}$;$Kras^{G12D}$;$R26R^{YFP}$ ($Kras^{G12D\text{-Duct}}$; n = 14; sourced from Kopp et al[22]), and 6- to 12-month-old $Sox9CreER^{T2}$;$Pten^{flox/+}$;$R26R^{YFP}$ ($Pten^{\Delta Duct/+}$) (n=5) mice. (*L*) Immunohistochemistry for PTEN in $Kras^{G12D}$;$Pten^{\Delta Duct/+}$ pancreata reveals reduced signal in tumor epithelium (arrows) and pancreatobiliary IPMN (asterisk). (*M*) Representative PCR analysis of *Pten* in DNA from normal or IPMN/tumor areas of a $Kras^{G12D}$;$Pten^{\Delta Duct/+}$ mouse. Scale bars: 5 mm (*C, D* and *G, H*), 500 μm (*E, I*), and 100 μm (*F, J,* and *L*).

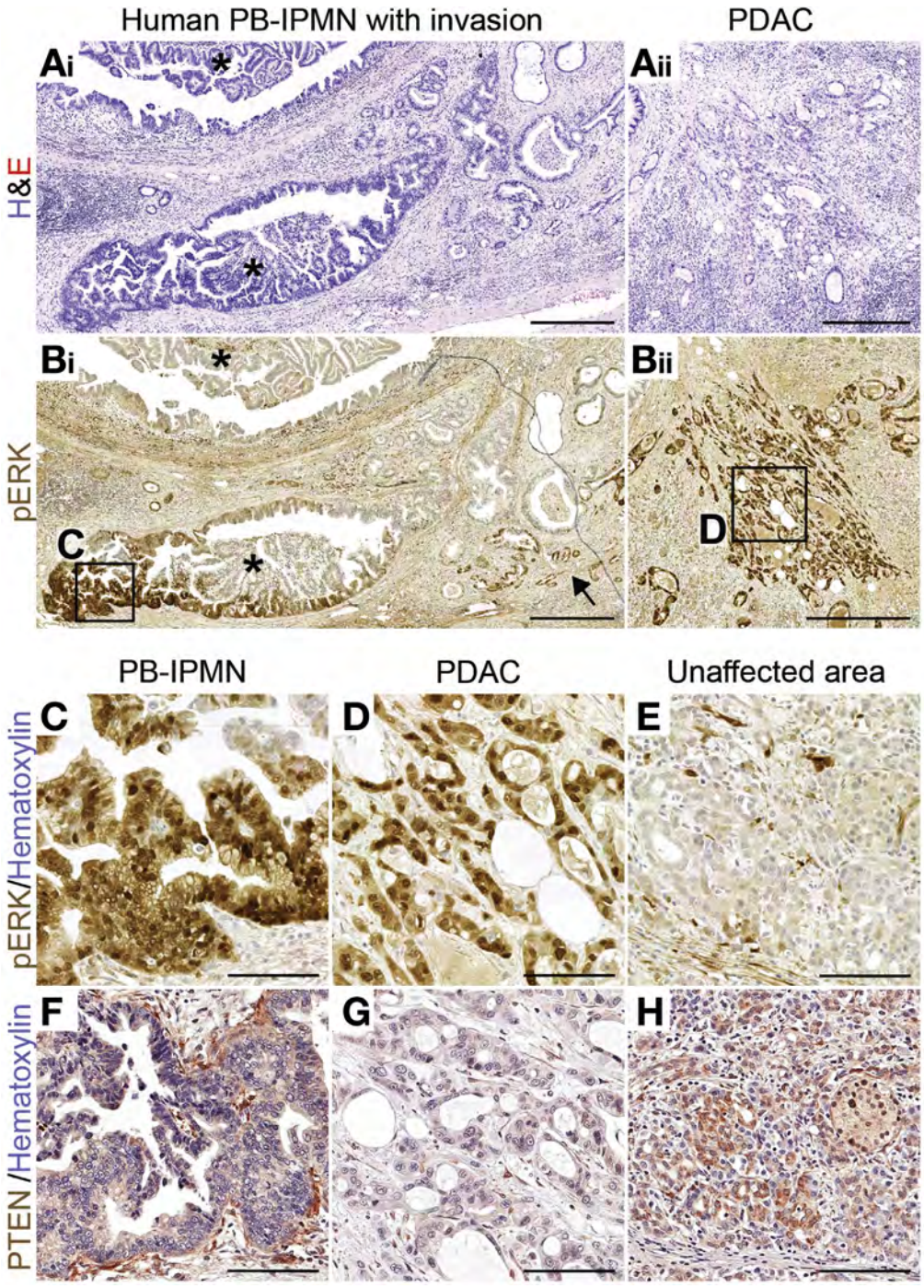

Figure 6. Activation of ERK and loss of PTEN are associated with progression of pancreatobiliary IPMN in humans. (*Ai–H*) Hematoxylin/eosin (H&E) (*Ai, Aii*) and immunohistochemistry for pERK (*Bi, Bii* and *C–E*) and PTEN (*F–H*) on sections of human pancreatobiliary IPMN (*Ai, Bi, C*, and *F*) and associated PDAC (*Aii, Bii, D*, and *G*). Asterisks in *Ai* and *Bi* indicate the IPMN and arrow in *Bi* indicates invasive glands directly associated with the IPMN. Boxed areas in *Bi* and *Bii* are magnified in *C* and *D*, respectively. PTEN staining for the same area as in *C* and *D* is shown on nearby sections in *F* and *G*. pERK (*E*) and PTEN (*H*) staining in unaffected areas of the same section. Scale bars: 500 μm (*Ai, Aii, Bi*, and *Bii*) and 100 μm (*C–H*).

no discernable phenotype by 12 months of age (see controls in Figures 1 and 2). To test whether *Pten* reduction and oncogenic Kras have synergistic roles in ductal cell transformation, we examined mice carrying a deletion of one *Pten* allele and expressing $Kras^{G12D}$ in ductal cells ($Sox9\text{-}CreER^{T2}$;$Kras^{G12D}$;$Pten^{flox/+}$;$R26R^{YFP}$ mice, hereafter referred to as $Kras^{G12D}$;$Pten^{\Delta Duct/+}$ mice; Figure 5*A* and *B*). All 30 analyzed $Kras^{G12D}$;$Pten^{\Delta Duct/+}$ mice exhibited focal PanIN, pre-IPMN, and/or pancreatic or common duct IPMN between 4 and 8 months of age (Figure 5*G–K*; Supplementary Figure 5*E* and *M*; Supplementary Table 2). The average total number of lesions was also greater in $Kras^{G12D}$;$Pten^{\Delta Duct/+}$ than in $Kras^{G12D\text{-}Duct}$ ($Sox9CreER^{T2}$;$Kras^{G12D}$;$R26R^{YFP}$) or $Pten^{\Delta Duct/+}$ mice (Figure 5*K* and Supplementary Table 1). Moreover, 21 of the 30 $Kras^{G12D}$;$Pten^{\Delta Duct/+}$ mice developed invasive PDAC that was associated with PanIN, pre-IPMN, or IPMN lesions (Figure 5*G–J*; Supplementary Figure 5*E* and *M*; Supplementary Table 1). These findings identify PTEN as a negative regulator of $Kras^{G12D}$-mediated ductal cell transformation.

Concomitant Kras Activation and Reduced Pten Induces Pancreatobiliary and Mixed Pancreatobiliary/Gastric Subtype IPMN

In humans, *KRAS* mutations are commonly found in both pancreatobiliary and gastric IPMN subtypes and rarely in O-IPMN.[9,10,26] To determine whether Ras activation impacts IPMN subtype identity, we analyzed pancreatic histology and mucin expression in $Kras^{G12D}$;$Pten^{\Delta Duct/\Delta Duct}$ and $Kras^{G12D}$;$Pten^{\Delta Duct/+}$ mice. IPMN-like lesions in $Kras^{G12D}$;$Pten^{\Delta Duct/\Delta Duct}$ mice exhibited histological features of the pancreatobiliary IPMN (Figure 5*E* and *F*; Supplementary Figure 5*A*, curved double-headed arrow), expressed the YFP lineage marker and were Muc1-positive, but Muc2-negative (Supplementary Figure 5*B–D*). However, some $YFP^{+}Muc1^{+}Muc2^{-}$ papillae also contained gastric-type epithelium (Supplementary Figure 5*I–L*) similar to the mixed gastric/pancreatobiliary IPMN subtype in humans.[3,27] Although gastric and pancreatobiliary papillae were roughly equally represented in IPMN-like lesions of $Kras^{G12D}$;$Pten^{\Delta Duct/\Delta Duct}$ mice, IPMN-like lesions in $Kras^{G12D}$;$Pten^{\Delta Duct/+}$ mice were primarily pancreatobiliary (Figure 5*H–J*; Supplementary Figure 5*E–H*; and Supplementary Table 1). Gastric epithelium in $Kras^{G12D}$;$Pten^{\Delta Duct/+}$ mice mostly met the histological and molecular criteria of microscopic PanIN rather than IPMN or pre-IPMN (Supplementary Figure 5*M–P*, show rare gastric or gastric/pancreatobiliary IPMN, and Supplementary Table 1). Different from $Pten^{\Delta Duct/\Delta Duct}$ mice, oncocytic IPMN were observed in neither $Kras^{G12D}$;$Pten^{\Delta Duct/+}$ nor $Kras^{G12D}$;$Pten^{\Delta Duct/\Delta Duct}$ mice. Together, these findings show that combined Kras activation and reduced *Pten* dosage predisposes ductal cells to form pancreatobiliary and gastric, but not oncocytic, IPMN. Thus, it appears that the presence of oncogenic Kras during IPMN induction can influence the IPMN subtype, providing a possible explanation for the low frequency of *KRAS* mutations in human oncocytic compared with gastric and pancreatobiliary IPMN.[3,9,26]

Loss of PTEN Underlies PDAC Development in $Kras^{G12D}$;$Pten^{\Delta Duct/+}$ Mice

In $Pten^{\Delta Duct/\Delta Duct}$ mice, *Kras* mutations were associated with invasion of pancreatobiliary IPMN (Figure 4*D* and Table 1), suggesting that complete *Pten* loss combined with Kras activation is needed for progression of pancreatobiliary IPMN. Consistent with this, pancreatobiliary-like papillae were associated with invasion into the stroma in all $Kras^{G12D}$;$Pten^{\Delta Duct/\Delta Duct}$ mice. In addition, at least 22 of the 33 pancreatobiliary IPMN lesions in $Kras^{G12D}$;$Pten^{\Delta Duct/+}$ mice were invasive. To test whether malignant progression of pancreatobiliary IPMN in $Kras^{G12D}$;$Pten^{\Delta Duct/+}$ mice is associated with spontaneous *Pten* loss, we analyzed PTEN expression in $Kras^{G12D}$;$Pten^{\Delta Duct/+}$ pancreatic tissue (n = 8). We found variable levels of PTEN signal in preneoplastic lesions and higher levels in tumor stroma, but little to no PTEN signal in pancreatobiliary IPMN-associated PDAC (Figure 5*L* and Supplementary Table 1). PCR for the $Pten^{flox}$, recombined-$Pten^{flox}$, or *Pten* wild-type alleles on IPMN lesions and associated PDAC revealed loss of the *Pten* wild-type allele in the IPMN/tumor in 2 of 8 $Kras^{G12D}$;$Pten^{\Delta Duct/+}$ mice (Figure 5*M* and Supplementary Table 1), showing loss of heterozygosity as a possible mechanism of PTEN protein loss. These findings support the conclusion that Kras activation combined with loss of PTEN promotes development of invasive pancreatobiliary IPMN. Furthermore, our data indicate that these events could occur in any order and appear to be positively selected for during progression of pancreatobiliary IPMN to PDAC.

Human Invasive Pancreatobiliary IPMN Exhibit Ras Signaling Activation and PTEN Loss

Loss of PTEN expression occurs in human PDAC[28] and is associated with poor prognosis of IPMN;[4] however, the relationship between PTEN loss and activation of KRAS in human pancreatobiliary IPMN is unclear. To examine whether PTEN loss and KRAS activation occurs in invasive human pancreatobiliary IPMN, we analyzed a case of human pancreatobiliary IPMN (Figure 6*Ai*, asterisks) with associated PDAC (Figure 6*Aii*) for pERK (Figure 6*Bi–E*) and PTEN (Figure 6*F–H*) expression. PTEN signal in both the IPMN and associated PDAC was reduced (Figure 6*F* and *G*) compared with the surrounding stroma (Figure 6*F*) and unaffected areas (Figure 6*H*). pERK signal was present in a portion of the IPMN (Figure 6*Bi*, boxed area magnified in 6*C*), the invasive glands (Figure 6*Bi*, arrow), and the IPMN-associated PDAC (Figure 6*Bii*, boxed area magnified in Figure 6*D*). This case study suggests that PTEN reduction is associated with IPMN development, but strong activation of RAS signaling with progression to invasive PDAC. Thus, as in our mouse models, both KRAS activation and PTEN loss appear to be associated with invasive pancreatobiliary IPMN in humans.

Discussion

We show here that PTEN loss with or without activation of Ras signaling in pancreatic ductal cells of mice recapitulates many clinicopathological features of human main-duct IPMN. In contrast to previously described mouse models exhibiting IPMN,[11–15] $Pten^{\Delta Duct/\Delta Duct}$ and $Kras^{G12D}$;$Pten^{\Delta Duct/+}$ mice developed macroscopic, focal lesions within the ductal tree, spontaneously acquired secondary genetic mutations, and progressed to PDAC in the context of predominantly normal pancreatic parenchyma. These features are similar to the stochastic formation of precancerous lesions and tumors presumed to underlie PDAC development in humans.

Similar to human IPMN, our mouse models developed solid, isolated nodules on the walls of enlarged ducts (like mural nodules) in the absence of widespread tissue changes. The presence of a mural nodule is a clinically relevant criterion for assessing the malignant potential of a human pancreatic cyst.[3,29] Because nodules in $Pten^{\Delta Duct/\Delta Duct}$ mice become invasive, this mouse model could help define additional events leading to the transformation of IPMN into PDAC. Furthermore, we observed IPMN lesions of multiple different subtypes, namely pancreatobiliary and oncocytic IPMN in $Pten^{\Delta Duct/\Delta Duct}$ mice and pancreatobiliary and gastric IPMN in $Kras^{G12D}$;$Pten^{\Delta Duct/+}$ mice. The IPMN subtypes in our mouse models showed characteristics highly similar to subtype-specific features observed in human IPMN. First,

mutation biases observed in human IPMN were recapitulated in our mouse models. Specifically, consistent with *Kras* mutations being rare in human oncocytic IPMN,[9,10,26] $Kras^{G12D}$ mutations or highly active Erk signaling were not detected in oncocytic IPMN of $Pten^{\Delta Duct/\Delta Duct}$ mice. Furthermore, *Kras* mutations were associated with gastric and pancreatobiliary IPMN in our mouse models, which is consistent with the higher rate of *KRAS* mutations in these subtypes in humans.[9,26] Second, $Kras^{G12D}$;$Pten^{\Delta Duct/+}$ mice displayed pancreatobiliary IPMN or pre-IPMN nodules that were continuous with gastric-type epithelium along the large pancreatic ducts. A highly similar phenomenon has been observed in multiple subtypes of human IPMN, which has led to the hypothesis that the gastric phenotype is the "null" phenotype and precedes the formation of other IPMN subtypes.[27] The $Kras^{G12D}$;$Pten^{\Delta Duct/+}$ model now presents an opportunity to dissect whether these lesions have a shared lineage or whether the gastric epithelium arises secondarily to the IPMN lesion. Given the impact of IPMN subtype identity on clinical prognosis,[2,3] dissecting the mechanisms that underlie initiation and progression of distinct IPMN subtypes could pave the way for the development of subtype-specific therapies of IPMN-PDAC.

Previous studies have shown that *Pten* inactivation in embryonic pancreatic precursor cells leads to expansion of centroacinar cells and ultimately progression to PDAC.[30] In contrast, we found that postnatal *Pten* deletion in ductal cells, including centroacinar cells, preferentially stimulated proliferation of cells in large ducts and had little effect on centroacinar cells. Similarly, combined *Pten* deletion and expression of oncogenic Kras in embryonic pancreatic precursor cells failed to induce IPMN,[28,31] in stark contrast to our observation after *Pten* deletion and Kras activation in postnatal ductal cells. Moreover, we found that IPMN formed only in response to ductal cell–specific, but not acinar cell–specific, *Pten* deletion. These observations illustrate that the phenotype caused by PDAC-associated genetic mutations is highly context-dependent. Therefore, inducing genetic mutations associated with human PDAC in specific cell types will help generate informative animal models to delineate the mechanistic underpinnings of human PDAC.

We demonstrate a ductal origin of IPMN lesions and associated PDAC in our genetic models. The similarity of the $Pten^{\Delta Duct/\Delta Duct}$ model to human IPMN suggests that a spontaneous loss of PTEN in ductal cells during adult life could predispose to IPMN. This idea is consistent with human studies showing that mutations in the PTEN/PI3K pathway are more common in IPMN-associated PDAC than in conventional PDAC.[4–8] However, not all $Kras^{G12D}$;$Pten^{\Delta Duct/+}$ mice showed *Pten* loss of heterozygosity. It is possible that posttranslational or epigenetic silencing mechanisms could also lead to PTEN loss, as shown in other contexts.[32] Further study of potential mechanisms underlying PTEN loss in IPMN-associated PDAC is clearly necessary. Here, cell lines derived from human or mouse IPMN-PDAC could help define molecular mechanisms.

We further observed synergy between reduced *Pten* dosage and Kras activation in IPMN formation from ductal cells and progression to PDAC. The most established function of PTEN is to restrain activity of the PI3K signaling pathway. PI3K is also activated by Ras signaling, arguing that high PTEN activity in ductal cells could suppress the transformative effects of oncogenic Kras. Consistent with this idea, ductal cell–specific expression of $Kras^{G12D}$ in the context of wild-type *Pten* had surprisingly little effect; the induction of a limited number of PanIN lesions in a subset of $Kras^{G12D}$-expressing mice being the only abnormality.[22] Here we observed more efficient induction of PanIN, pre-IPMN, and IPMN when $Kras^{G12D}$ was expressed in the context of reduced PTEN, showing that PTEN indeed counteracts effects of oncogenic Kras in ductal cells. If the combined acquisition of PTEN loss and RAS activation we observed in a case of human pancreatobiliary IPMN-PDAC was verified in a larger number of cases, these features could become markers to distinguish IPMN with high and low malignant potential to inform patient selection for therapeutic intervention. In fact, reducing hyperinsulinemia-induced PI3K signaling through lifestyle modifications or pharmaceutical inhibition could reduce the risks of IPMN progression. Further studies examining how closely these mouse models recapitulate molecular aspects of human disease with regard to the accumulation of other IPMN-associated genetic and transcriptional changes could enable discovery of additional drivers of IPMN initiation and malignant progression.

Supplementary Information

Supplementary information includes 5 figures and 2 tables.

Supplementary Material

Note: To access the supplementary material accompanying this article, visit the online version of *Gastroenterology* at www.gastrojournal.org, and at https://doi.org/10.1053/j.gastro.2017.12.007.

References

1. Grutzmann R, Niedergethmann M, Pilarsky C, et al. Intraductal papillary mucinous tumors of the pancreas: biology, diagnosis, and treatment. Oncologist 2010; 15:1294–1309.
2. Distler M, Kersting S, Niedergethmann M, et al. Pathohistological subtype predicts survival in patients with intraductal papillary mucinous neoplasm (IPMN) of the pancreas. Ann Surg 2013;258:324–330.
3. Adsay V, Mino-Kenudson M, Furukawa T, et al. Pathologic evaluation and reporting of intraductal papillary mucinous neoplasms of the pancreas and other tumoral intraepithelial neoplasms of pancreatobiliary tract: recommendations of Verona Consensus Meeting. Ann Surg 2016;263:162–177.
4. Garcia-Carracedo D, Turk AT, Fine SA, et al. Loss of PTEN expression is associated with poor prognosis in patients with intraductal papillary mucinous neoplasms of the pancreas. Clin Cancer Res 2013;19:6830–6841.
5. Mohri D, Asaoka Y, Ijichi H, et al. Different subtypes of intraductal papillary mucinous neoplasm in the pancreas have distinct pathways to pancreatic cancer progression. J Gastroenterol 2012;47:203–213.

6. Samuels Y, Wang Z, Bardelli A, et al. High frequency of mutations of the PIK3CA gene in human cancers. Science 2004;304:554.
7. Schonleben F, Qiu W, Ciau NT, et al. PIK3CA mutations in intraductal papillary mucinous neoplasm/carcinoma of the pancreas. Clin Cancer Res 2006;12:3851–3855.
8. Lubezky N, Ben-Haim M, Marmor S, et al. High-throughput mutation profiling in intraductal papillary mucinous neoplasm (IPMN). J Gastrointest Surg 2011; 15:503–511.
9. Kuboki Y, Shimizu K, Hatori T, et al. Molecular biomarkers for progression of intraductal papillary mucinous neoplasm of the pancreas. Pancreas 2015;44:227–235.
10. **Wu J, Matthaei H**, Maitra A, et al. Recurrent GNAS mutations define an unexpected pathway for pancreatic cyst development. Sci Transl Med 2011;3:92ra66.
11. Siveke JT, Einwächter H, Sipos B, et al. Concomitant pancreatic activation of Kras(G12D) and Tgfa results in cystic papillary neoplasms reminiscent of human IPMN. Cancer Cell 2007;12:266–279.
12. **Bardeesy N, Cheng KH**, Berger JH, et al. Smad4 is dispensable for normal pancreas development yet critical in progression and tumor biology of pancreas cancer. Genes Dev 2006;20:3130–3146.
13. **Vincent DF, Yan KP**, Treilleux I, et al. Inactivation of TIF1gamma cooperates with Kras to induce cystic tumors of the pancreas. PLoS Genet 2009;5:e1000575.
14. **von Figura G, Fukuda A, Roy N**, et al. The chromatin regulator Brg1 suppresses formation of intraductal papillary mucinous neoplasm and pancreatic ductal adenocarcinoma. Nat Cell Biol 2014;16:255–267.
15. Qiu W, Tang SM, Lee S, et al. Loss of activin receptor type 1B accelerates development of intraductal papillary mucinous neoplasms in mice with activated KRAS. Gastroenterology 2016;150:218–228.e12.
16. Font-Burgada J, Shalapour S, Ramaswamy S, et al. Hybrid periportal hepatocytes regenerate the injured liver without giving rise to cancer. Cell 2015;162:766–779.
17. Kopinke D, Brailsford M, Pan FC, et al. Ongoing Notch signaling maintains phenotypic fidelity in the adult exocrine pancreas. Dev Biol 2012;362:57–64.
18. Lesche R, Groszer M, Gao J, et al. Cre/loxP-mediated inactivation of the murine Pten tumor suppressor gene. Genesis 2002;32:148–149.
19. Tuveson DA, Shaw AT, Willis NA, et al. Endogenous oncogenic K-ras(G12D) stimulates proliferation and widespread neoplastic and developmental defects. Cancer Cell 2004;5:375–387.
20. Srinivas S, Watanabe T, Lin CS, et al. Cre reporter strains produced by targeted insertion of EYFP and ECFP into the ROSA26 locus. BMC Dev Biol 2001;1:4.
21. Taylor BL, Liu FF, Sander M. Nkx6.1 is essential for maintaining the functional state of pancreatic beta cells. Cell Rep 2013;4:1262–1275.
22. **Kopp JL, von Figura G**, Mayes E, et al. Identification of Sox9-dependent acinar-to-ductal reprogramming as the principal mechanism for initiation of pancreatic ductal adenocarcinoma. Cancer Cell 2012;22:737–750.
23. Jiao J, Wang S, Qiao R, et al. Murine cell lines derived from Pten null prostate cancer show the critical role of PTEN in hormone refractory prostate cancer development. Cancer Res 2007;67:6083–6091.
24. Jackson JB, Choi DS, Luketich JD, et al. Multiplex preamplification of serum DNA to facilitate reliable detection of extremely rare cancer mutations in circulating DNA by digital PCR. J Mol Diagn 2016; 18:235–243.
25. **Westmoreland JJ, Drosos Y**, Kelly J, et al. Dynamic distribution of claudin proteins in pancreatic epithelia undergoing morphogenesis or neoplastic transformation. Dev Dyn 2012;241:583–594.
26. Furukawa T, Kuboki Y, Tanji E, et al. Whole-exome sequencing uncovers frequent GNAS mutations in intraductal papillary mucinous neoplasms of the pancreas. Sci Rep 2011;1:161.
27. Adsay NV, Merati K, Basturk O, et al. Pathologically and biologically distinct types of epithelium in intraductal papillary mucinous neoplasms: delineation of an "intestinal" pathway of carcinogenesis in the pancreas. Am J Surg Pathol 2004;28:839–848.
28. Ying H, Elpek KG, Vinjamoori A, et al. PTEN is a major tumor suppressor in pancreatic ductal adenocarcinoma and regulates an NF-kappaB-cytokine network. Cancer Discov 2011;1:158–169.
29. Anand N, Sampath K, Wu BU. Cyst features and risk of malignancy in intraductal papillary mucinous neoplasms of the pancreas: a meta-analysis. Clin Gastroenterol Hepatol 2013;11:913–921; quiz e59–e60.
30. Stanger BZ, Stiles B, Lauwers GY, et al. Pten constrains centroacinar cell expansion and malignant transformation in the pancreas. Cancer Cell 2005;8:185–195.
31. Hill R, Calvopina JH, Kim C, et al. PTEN loss accelerates KrasG12D-induced pancreatic cancer development. Cancer Res 2010;70:7114–7124.
32. **Correia NC, Girio A, Antunes I**, et al. The multiple layers of non-genetic regulation of PTEN tumour suppressor activity. Eur J Cancer 2014;50:216–225.

Author names in bold designate shared co-first authorship.

Received March 20, 2017. Accepted December 14, 2017.

Reprint requests
Address requests for reprints to: Maike Sander, MD, Departments of Pediatrics and Cellular and Molecular Medicine, University of California-San Diego, La Jolla, California 92093-0695. e-mail: masander@ucsd.edu; fax: (858) 822-3249.

Acknowledgments
We thank Nissi Varki (University of California, San Diego Cancer Center, Histopathology Core), Fenfen Liu, Nancy Rosenblatt, Sangho Yu, Manbir Sandhu, Brandon Taylor, and Yu Cao for expert technical assistance, and the University of California, San Diego, Electron Microscopy Core for image preparation. We are grateful to Andrew Lowy for advice, members of the Sander and Kopp laboratories for discussions, and Andrea C. Carrano for help with preparation of the manuscript. We thank Christopher Wright (Vanderbilt University) for *Ptf1a*^{CreER} mice and David Tuveson (Cold Spring Harbor Laboratory) for *LSL-Kras*^{G12D} mice.

Conflicts of interest
The authors declare no competing interests in the present study.

Funding
This work was supported by National Institutes of Health (NIH) grants R01DK078803 and R21CA194839 to Maike Sander; NIH-F32CA136124 and Canadian Institutes of Health Research Operating Grant and New Investigator Award to Janel L. Kopp; and Cancer Prevention Research Institute of Texas Rising Stars Award, University of Texas Stars Grant, and R01 CA136526 to Andrew D. Rhim.

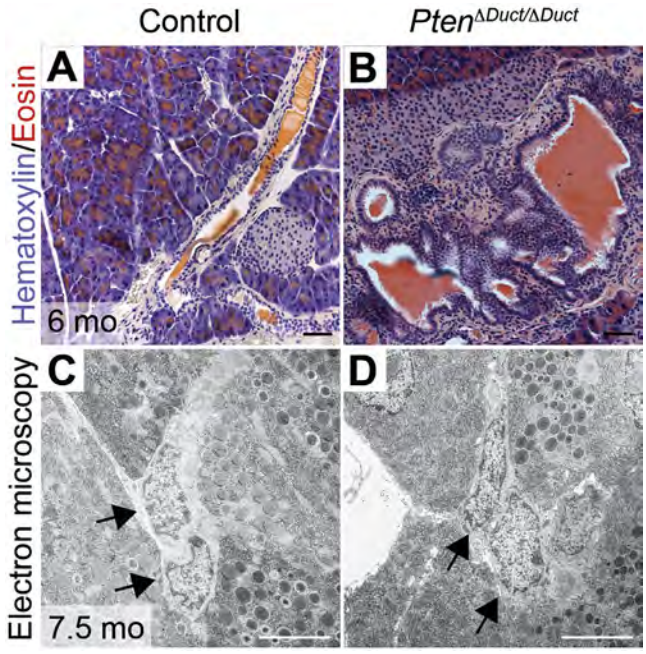

Supplementary Figure 1. *Pten* deletion in pancreatic ductal cells results in large, but not small duct, hyperplasia. (*A, B*) Hematoxylin/eosin staining reveals hyperplasia of the large pancreatic duct in 6-month-old $Pten^{\Delta Duct/\Delta Duct}$, but not control, mice. (*C, D*) Electron micrographs of centroacinar/terminal duct cells (arrows) in 7.5-month-old control and $Pten^{\Delta Duct/\Delta Duct}$ mice. Scale bars: 50 μm (*A, B*), and 5 μm (*C, D*).

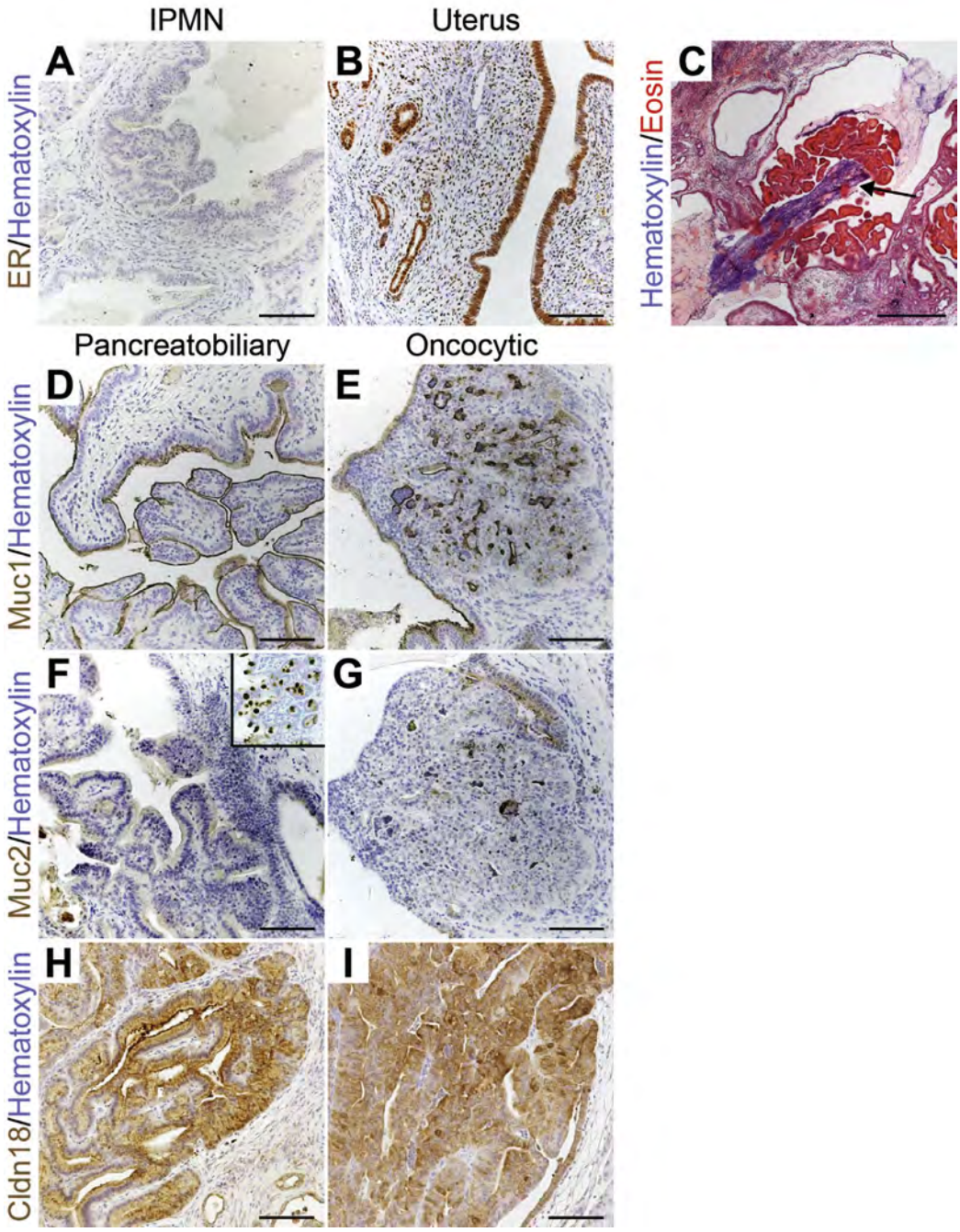

Supplementary Figure 2. Ductal lesions in *Pten*$^{\Delta Duct/\Delta Duct}$ mice express molecular markers of IPMN, but not MCN. (*A, B*) Immunohistochemistry for the estrogen receptor shows absence of MCN-associated estrogen receptor–positive ovarian-type stroma in lesions from *Pten*$^{\Delta Duct/\Delta Duct}$ mice (*A*). Uterine tissue (*B*) was used as a positive control. (*C*) Hematoxylin/eosin staining showing mucin accumulation (arrow) in the lumen of an enlarged pancreatic duct. (*D–I*) Immunohistochemistry for Muc1 (*D, E*), Muc2 (*F, G*), and Claudin 18 (Cldn18) (*H, I*) reveals similarity of IPMN-like lesions in *Pten*$^{\Delta Duct/\Delta Duct}$ mice to the pancreatobiliary (*D, F, H*) and oncocytic (*E, G, I*) subtypes of IPMN. Inset in (*F*) shows levels of Muc2 staining in intestinal goblet cells as a positive control. Scale bars: 100 μm (*A, B, D–I*) and 500 μm (*C*).

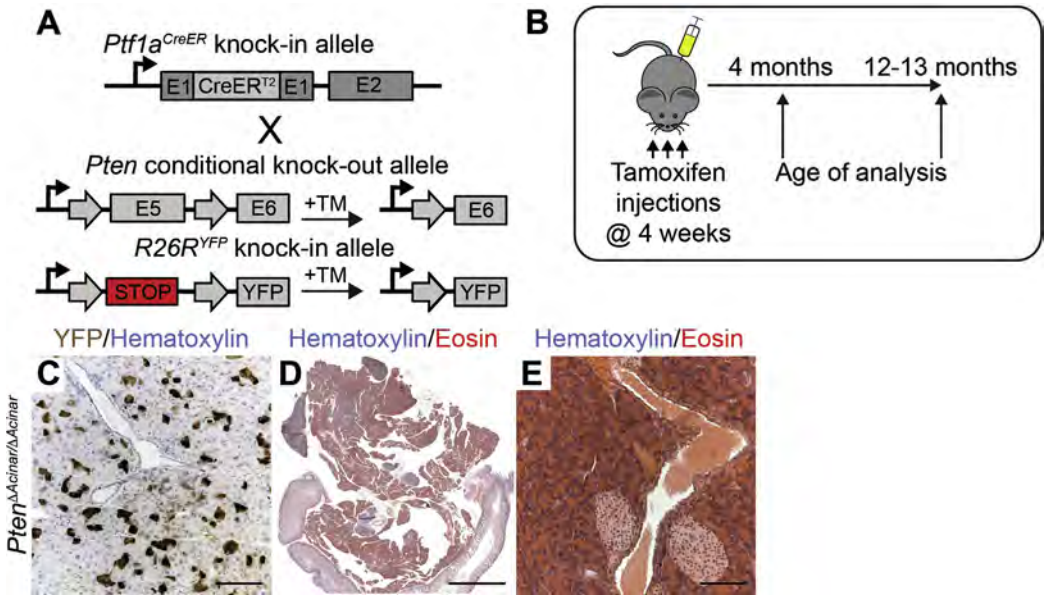

Supplementary Figure 3. *Pten* deletion in acinar cells does not result in IPMN formation. *(A)* Strategy to generate *Ptf1a*^{CreER};*Pten*$^{flox/flox}$;*R26R*^{YFP} (*Pten*$^{\Delta Acinar/\Delta Acinar}$) mice. TM injection induces recombination of the *Pten*^{flox} and *R26R*^{YFP} alleles in *Ptf1a*-expressing cells. *(B)* *Pten*$^{\Delta Acinar/\Delta Acinar}$, *Pten*$^{\Delta Acinar/+}$, and *Ptf1a*^{CreER};*Pten*$^{+/+}$;*R26R*^{YFP} mice were injected with TM on postnatal days 28, 30, and 32 and analyzed at 4 or 12 to 13 months of age. *(C)* Immunohistochemistry for YFP in a *Pten*$^{\Delta Acinar/\Delta Acinar}$ mouse at 4 months of age. *(D, E)* A tiled *(D)* and higher magnification *(E)* image showing hematoxylin/eosin staining of a pancreatic section from a *Pten*$^{\Delta Acinar/\Delta Acinar}$ mouse at 12 months of age. Scale bars: 5 mm *(D)* and 100 μm *(C, E)*.

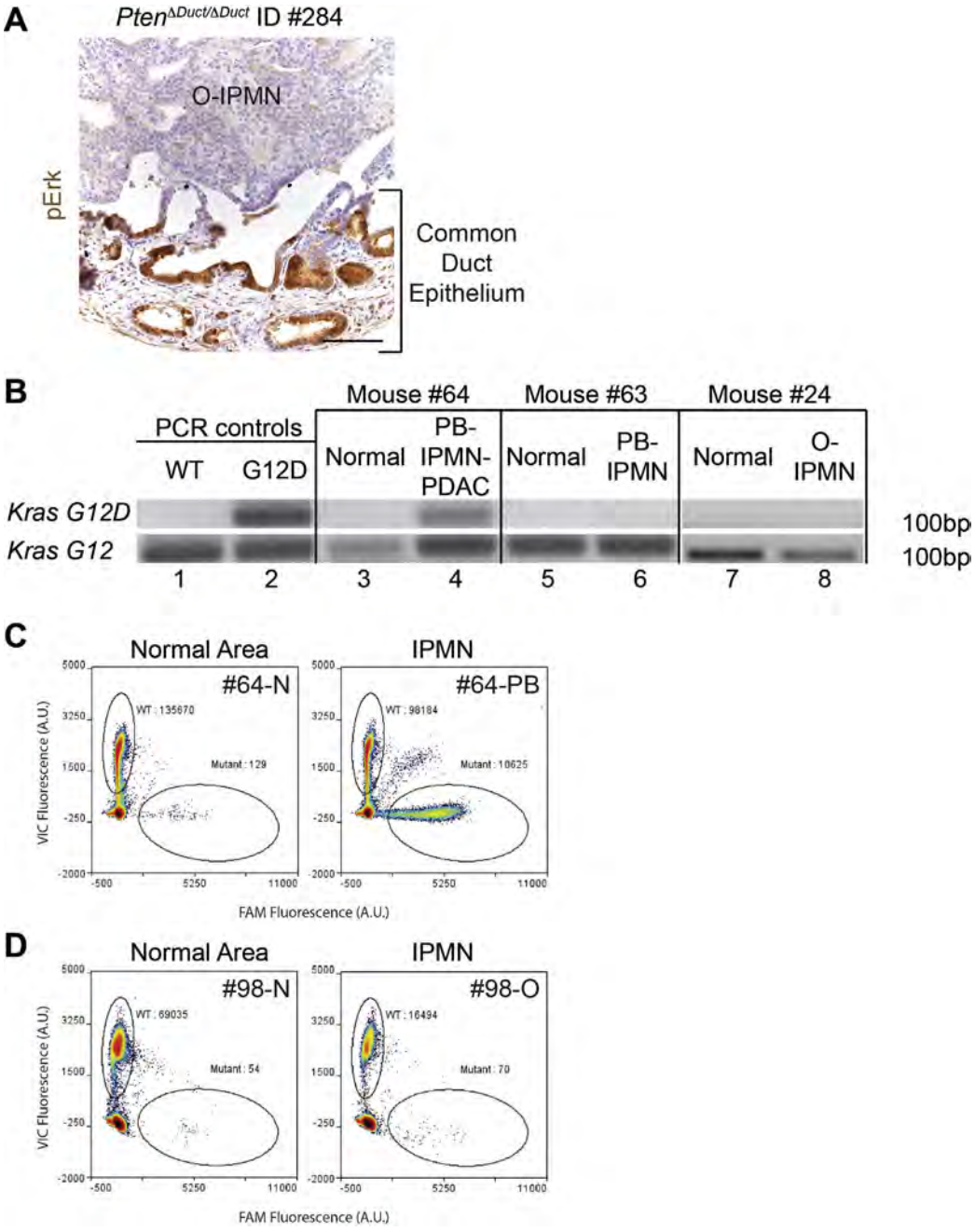

Supplementary Figure 4. *Kras* mutations associated with invasive pancreatobiliary IPMN in *Pten*$^{\Delta Duct/\Delta Duct}$ mice. (*A*) Immunohistochemistry for pErk on pancreatic sections of a 12-month-old *Pten*$^{\Delta Duct/\Delta Duct}$ mouse, identification number (ID) 284, with O-IPMN, showing that the wall of this cyst in the common duct is pErk-positive. (*B*) Allele-specific PCR to detect mouse *KrasG12D* (top) *or KrasG12* (bottom). Across the gel: Genomic DNA from wild-type (WT) (column 1) and *LSL-Kras*^{G12D} mice (G12D) (column 2), from a nontumor area (Normal) (column 3) and an invasive pancreatobiliary IPMN with associated tumor (PB-IPMN-PDAC) (column 4) in *Pten*$^{\Delta Duct/\Delta Duct}$ mouse #64, from normal pancreas (Normal) (column 5) and a noninvasive pancreatobiliary IPMN (PB-IPMN) (column 6) in *Pten*$^{\Delta Duct/\Delta Duct}$ mouse #63, from normal pancreas (Normal) (column 7) and a noninvasive O-IPMN (column 8) in *Pten*$^{\Delta Duct/\Delta Duct}$ mouse #24. (*C, D*) Multiplexed droplet digital PCR to detect *Kras* mutations in normal (left plots) or IPMN-containing (right plots) tissue from *Pten*$^{\Delta Duct/\Delta Duct}$ mice, identification numbers 64 and 98. Mutant *Kras* alleles are detected with FAM-labeled probes, whereas VIC-labeled probes detect the WT allele. Scale bar: 100 μm (*A*).

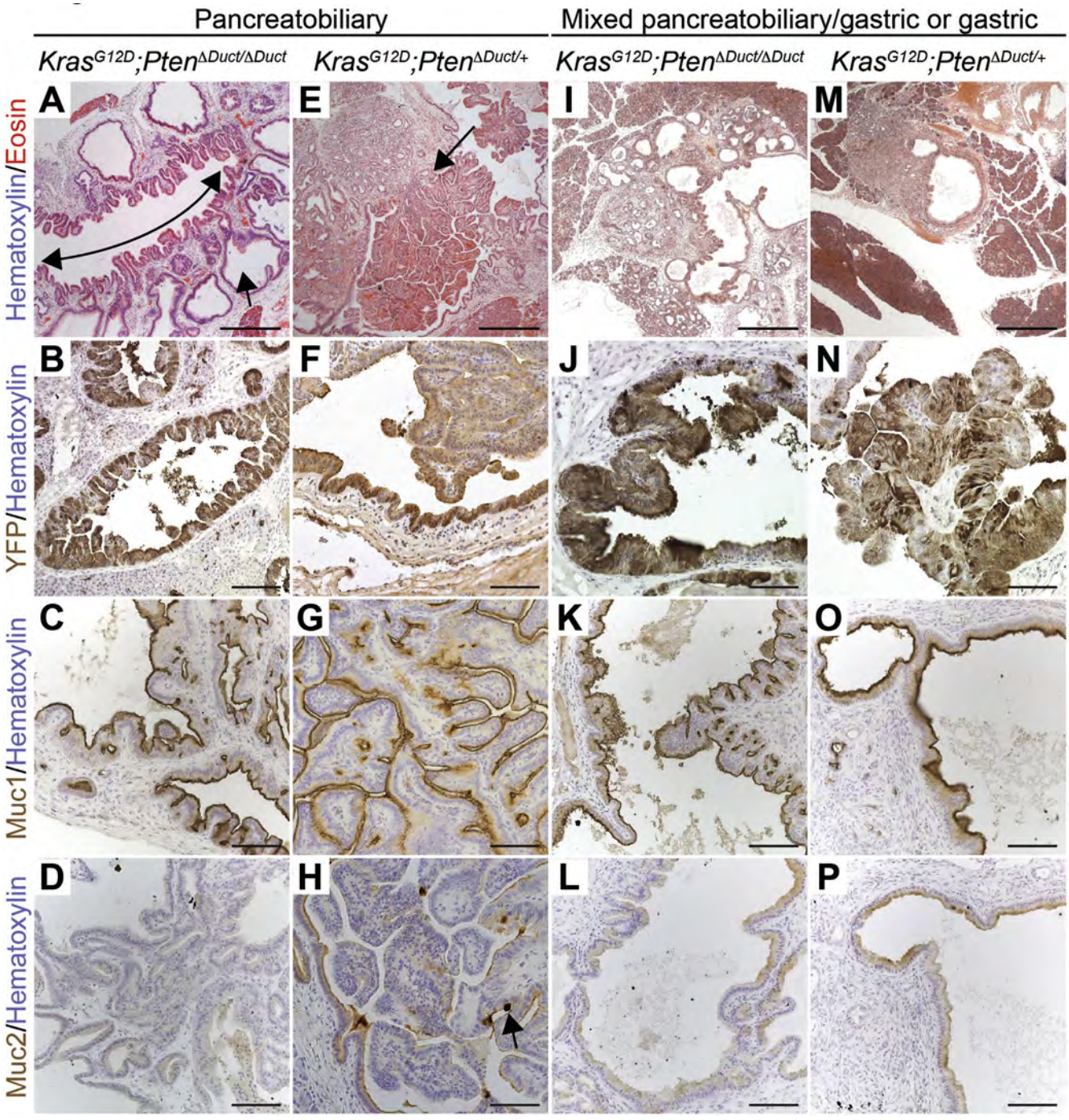

Supplementary Figure 5. *Pten* reduction combined with oncogenic Kras induces pancreatobiliary and gastric IPMN lesions. Hematoxylin/eosin (*A, E, I,* and *M*) and immunohistochemistry for YFP (*B, F, J,* and *N*), Muc1 (*C, G, K,* and *O*), and Muc2 (*D, H, L,* and *P*) on sections of pancreatobiliary (*A–H*) or mixed pancreatobiliary/gastric and gastric IPMN (*I–P*) in $Kras^{G12D};Pten^{\Delta Duct/\Delta Duct}$ and $Kras^{G12D};Pten^{\Delta Duct/+}$ mice. Double-sided curved arrow in (*A*) indicates extensive papillary protrusions along the lumen of the common duct. Arrow in (*A*) indicates an enlarged peribiliary gland. Arrow in (*E*) denotes the point where a focal IPMN lesion arose from the ductal epithelium. The associated PDAC is basal to this spot. Arrow in (*H*) indicates the level of Muc2 staining in rare goblet cells in the IPMN lesions, shown as an internal positive control. Scale bars: 500 μm (*A, E, I,* and *M*) and 100 μm (*B–D, F–H, J–L*, and *N–P*).